IEEE Access
Multidisciplinary | Rapid Review | Open Access Journal

SPECIAL SECTION ON ADVANCED ENERGY CONVERSION SYSTEMS BASED ON MULTI-PORT ELECTRICAL MACHINES

Received August 12, 2021, accepted September 1, 2021, date of publication September 3, 2021,
date of current version September 13, 2021.

Digital Object Identifier 10.1109/ACCESS.2021.3110373

Recent Advances of Control Technologies for Brushless Doubly-Fed Generators

YI LIU[1,2], (Senior Member, IEEE),
MOHAMED G. HUSSIEN[3], (Graduate Student Member, IEEE),
WEI XU[1], (Senior Member, IEEE),
SHIYI SHAO[4], (Member, IEEE),
AND ESSAM M. RASHAD[3], (Senior Member, IEEE)

[1]State Key Laboratory of Advanced Electromagnetic Engineering and Technology, School of Electrical and Electronic Engineering, Huazhong University of Science and Technology (HUST), Wuhan 430074, China
[2]High-Efficiency and Energy-Saving Electrical Machine R&D Center of HUST, Zibo High-Tech Development Zone, Zibo 255100, China
[3]Department of Electrical Power and Machines Engineering, Faculty of Engineering, Tanta University, Tanta 31111, Egypt
[4]Wuxi Silent Electric System Technology Company Ltd., Wuxi 214000, China

Corresponding author: Wei Xu (weixu@hust.edu.cn)

This work was supported in part by the Excellent Youth Fund of Shandong Natural Science Foundation under Grant ZR2020YQ40, in part by the National Natural Science Foundation of China under Grant 51877093, in part by the National Key Research and Development Program of China under Grant 2018YFE0100200, in part by the Key Technical Innovation Program of Hubei Province under Grant 2019AAA026, in part by the Fund from Science, Technology and Innovation Commission of Shenzhen Municipality under Grant JCYJ20190809101205546, and in part by the Fundamental Research Funds for the Central Universities of China under Grant 2021XXJS002.

ABSTRACT The brushless doubly-fed generator (BDFG) is a kind of dual-electrical-port field-modulated electrical machine containing two sets of stator windings with different pole pairs. The stator power winding undertakes most of the power inflow and outflow, and the stator control winding connected to the power converter can be utilized to regulate the machine operation status. Consequently, the rotor no longer needs to be supplied by the power converter, so that the brushes and slip rings can be removed. The BDFG can be used for grid-connected power generation as well as standalone power generation. This paper reviews recent advances of control technologies for BDFGs under different operation conditions, e.g., grid-connected ac power generation with normal and faulty grids, standalone ac power generation with normal and special loads, and dc power generation. The progresses of sensorless control technologies for BDFG-based power generation systems are also discussed. The classification and comparison are carried out to discover the similarities and differences between theses control technologies. This paper is in the hope of inspiring new, ground breakings and progresses for high-performance BDFG power generator applications.

INDEX TERMS Brushless doubly-fed induction generator, ac power generation, dc power generation, grid-connected power generation, sensorless control, standalone power generation.

ABBREVIATIONS

BDFIG	Brushless doubly-fed induction generator
BDFRG	Brushless doubly-fed reluctance generator
CDFIG	Cascade doubly-fed induction generator
CW	Control winding
DFR	Dual frequency resonance
DPC	Direct power control
DSDBFIG	Dual-stator BDFIG
DSF	Dual synchronous frame
DSOGI	Dual second-order generalized integrators
DTC	Direct torque control
DVC	Direct voltage control
ISC	Indirect stator-quantities control
LSC	Line side converter
LVRT	Low-voltage ride-through
MPCC	Model predictive current control
MPFSO	Machine-parameter-free speed observer
MRAS	Model reference adaptive system
MSC	Machine side converter
MSOGI	Multiple second-order generalized integrators
NPCC	Nonparametric predictive current control

The associate editor coordinating the review of this manuscript and approving it for publication was Atif Iqbal.

PCC	Point of common coupling
PI	Proportional-integral
PIR	Proportional-integral-resonant
PR	Proportional-resonant
PW	Power winding
SDR	Series dynamic resistor
SFRF	Slip frequency rotating frame
SSF	Single synchronous frame
VC	Vector control

NOMENCLATURE

p_1, p_2	Pole pair numbers of PW and CW
ω_1, ω_2	Angular frequencies of PW and CW
θ_1, θ_2	Positions of PW voltage and CW current vectors
ω_r, θ_r	Angular speed and position of rotor
u, i, ψ	Voltage, current, and flux scalars
R_1, R_2, R_r	Resistances of PW, CW, and rotor
L_1, L_2, L_r	Self-inductances of PW, CW, and rotor
L_{1r}, L_{2r}	Coupling inductances between the stator and rotor windings
s	Differential operator, i.e., d/dt

Superscripts

$*$	Reference value
^	Estimated value

Subscripts

1, 2, r	PW, CW, and rotor
a, b, c	Phases a, b and c of three-phase voltage or current
α, β	Stationary $\alpha\beta$ axes
d, q	Synchronous rotating dq axes
f	Filtered quantity

I. INTRODUCTION

The high reliability structure gives the superiority to the brushless doubly-fed generator (BDFG) in the adjustable drive systems. The fixed stator frame of the BDFG contains two windings separated and isolated with different number of poles [1]. One of the two windings is specified as the main winding of the machine, which is denoted as the power winding (PW). The other winding is for control purpose and known as the control winding (CW). The two stator windings are with different pair poles to prevent the direct coupling between them. The role of the rotor is to couple the two fixed windings through indirect magnetic coupling. Unlike the conventional doubly-fed induction generator (DFIG), the rotor of the BDFG no longer needs to be supplied by the power converter, so that the brushes and slip rings associated with the rotor can be removed [2].

Based on [3] and [4], a fair comparison between the DFIG and BDFG is depicted in TABLE 1 to state the typical strengths and weaknesses of the two kinds of generators. In Table R1, the symbol "+" indicates the strength and the symbol "-" stands for the weakness. From TABLE 1, the BDFG is worse than the DFIG in terms of size and mass, efficiency, torque density and manufacture cost. Fortunately, the BDFG's weaknesses can be compensated by its higher mechanical reliability, lower maintenance cost and stronger low-voltage ride-through (LVRT) capability, due to the absence of brushes or slip-rings and the improved performance under faulty grids. These strengths of the BDFG are very important for practical industrial applications.

TABLE 1. Comparison of strengths and weaknesses between DFIG and BDFG [3], [4].

Metrics of interest	DFIG	BDFG
Size and mass	Small (+)	Large (-)
Efficiency	High (+)	Low (-)
Torque density	High (+)	Low (-)
Mechanical reliability	Low (-)	High (+)
Maintenance cost	High (-)	Low (+)
Manufacture cost	Low (+)	High (-)
LVRT capability	Low (-)	High (+)

The current BDFGs can be divided into two main categories, i.e., the single-stator BDFGs and the dual-stator BDFG. The single-stator BDFGs mainly include the brushless doubly-fed induction generator with nested-loop rotor (BDFIG-NLR) [5], [6], the brushless doubly-fed reluctance generator (BDFRG) [7], [8], the BDFIG with wound rotor (BDFIG-WR) [9], and the BDFG with hybrid rotor (BDFG-HR) [10]. The dual-stator BDFG mainly refers to the dual-stator BDFIG (DSBDFIG) proposed in [11].

At present, the types of BDFG-based power generation systems mainly include ac and dc power generation systems. The topology of the BDFG-based ac power generation system can be seen in Fig. 1. The employed power converter is composed of two back-to-back voltage source converters with a common dc bus, i.e., the machine side converter (MSC) and the line side converter (LSC). This topology can be used for both grid-connected and standalone power generation. The difference between the grid-connected and standalone power generation systems is that the point of common coupling (PCC) of the grid-connected system is connected to grid, while the PCC of the standalone system is connected to loads.

The grid-connected BDFG-based ac power generation system can be applied to variable speed constant frequency (VSCF) wind power and hydropower generation. The aim of this system is to regulate the active and reactive power of PW, which can be achieved by MSC. The LSC is employed to maintain the dc bus voltage constant regardless of power flow direction through MSC. Also, the LSC can be utilized to assist the fault ride-through under faulty grids.

The application scenarios of the standalone ac power generation system include wind power and hydro power in remote locations, portable variable speed power generation, ship shaft power generation, and so on. Unlike the grid-connected BDFG system, the control objective of the standalone BDFG is to make the amplitude and frequency of

PW voltage maintain constant under variable rotor speeds and loads. In the standalone system, the CW should be controlled by the MSC to build up a constant PW voltage to support the loads [12]. The main role of LSC is to keep the dc bus voltage stable, which is similar to the grid-connected system. The LSC can also assist in stabilizing the voltage fluctuation at the point of common coupling by supplying or absorbing reactive current as discussed in [13].

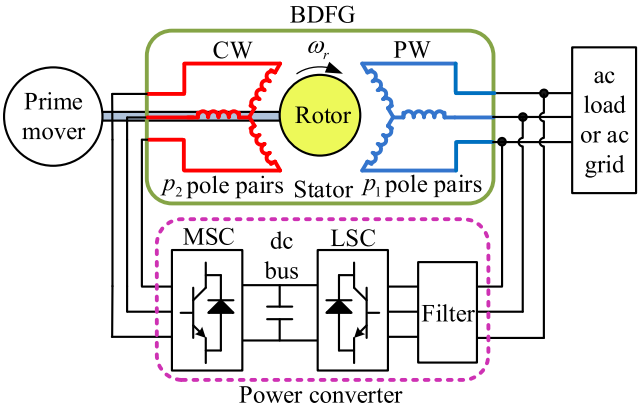

FIGURE 1. The topology of the BDFG-based ac power generation system.

The topology of the BDFG-based dc power generation system is shown in Fig. 2. The main difference between this system and the BDFG-based ac system is that the LSC is replaced by the diode rectifier [14]. Hence, the cost of the power converter can be significantly reduced. The output of this system can be connected to the dc grid or dc load. The BDFG-based dc power generation system can be used for wind power, hydro power, portable variable speed power generation and ship shaft power generation connected to dc grid or dc load. The control objective of the BDFG-based dc power generation system is to regulate the active power for grid-connected operation mode, and to adjust the dc bus voltage for standalone operation mode. In comparison with the ac power generation system, the control objective of the dc power generation system is much simpler. Besides, the PW voltage frequency is not necessary to be constant, since the sinusoidal PW voltage is converted to the dc voltage by the diode rectifier. Consequently, the frequency of PW voltage would be a free variable, which can be utilized to achieve more control objectives, e.g., efficiency optimization and speed range extension.

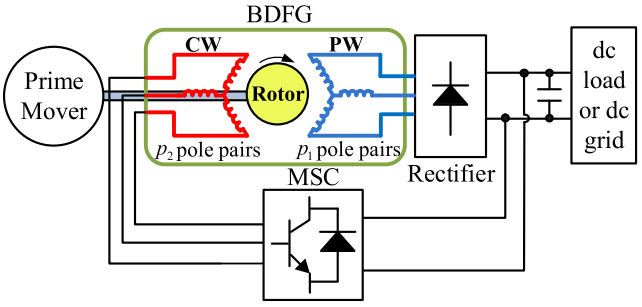

FIGURE 2. The topology of the BDFG-based dc power generation system.

The BDFG has been applied to wind power, ship shaft power and hydropower generation. According to the literature survey, in 2009, the BDFIG-NLR was applied to wind power generation for the first time [15]. As shown in Fig. 3, the BDFIG is mechanically coupled to the wind turbine via a speed-increasing gearbox. The tested BDFIG is with the rated power of 20 kW, the PW pole pair of 2 and the CW pole pair of 4. With the proposed control algorithm in [15], the efficiency of the tested BDFIG can be up to 80%.

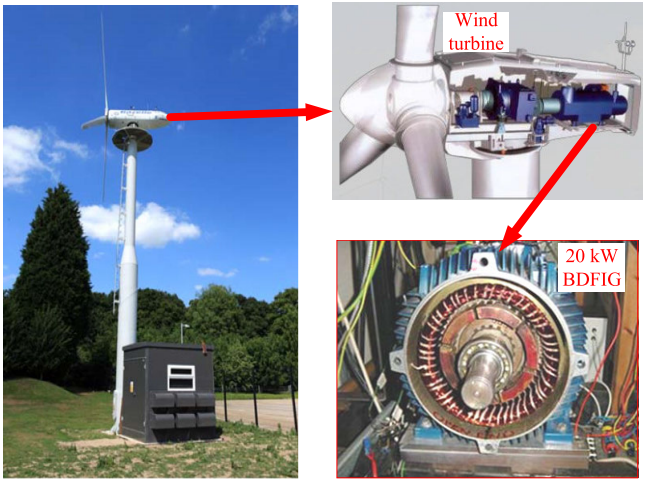

FIGURE 3. The BDFIG application in wind power generation [15].

The BDFIG can also be applied to the ship power system. In general, the power redundancies of commercial ships have a range of approximately 10%-15% from the main engine for shipping safety. During the cruise, the ship shaft generator can use this redundant power of the main engine for power generation, so that the efficiency of the main engine can be significantly improved and the use of diesel generator sets can be greatly reduced. As shown in Fig. 4, a typical ship shaft power generation system based on a 60-kW wound-rotor BDFIG has been tested in a 325 TEU container ship from the Changjiang National Shipping Group of China between 2011 and 2014, which can save 30% of the fuel cost of the ship at most [12].

A typical case of the BDFIG application in hydropower generation can be seen in [16]. As illustrated in Fig. 5, the wound-rotor BDFIG is mechanically coupled to a hydraulic turbine without gearbox. The applied BDFIG is with the rated power of 800 kW, and with the PW and CW rated voltages of 6.3 kV and 400 V, respectively. Hence, the PW can be directly connected the 6.3 kV high-voltage grid, and the CW has to be indirectly linked the same grid through the low-voltage back-to-back power converters and the transfer. Consequently, the high-voltage BDFIG can be regulated by the low-voltage power converters.

Lots of control technologies for BDFG-based ac and dc power generation systems have been developed toward industry applications in wind power, ship shaft power, hydropower, and so on. This paper will introduce recent advances of these control technologies, and investigate the similarities

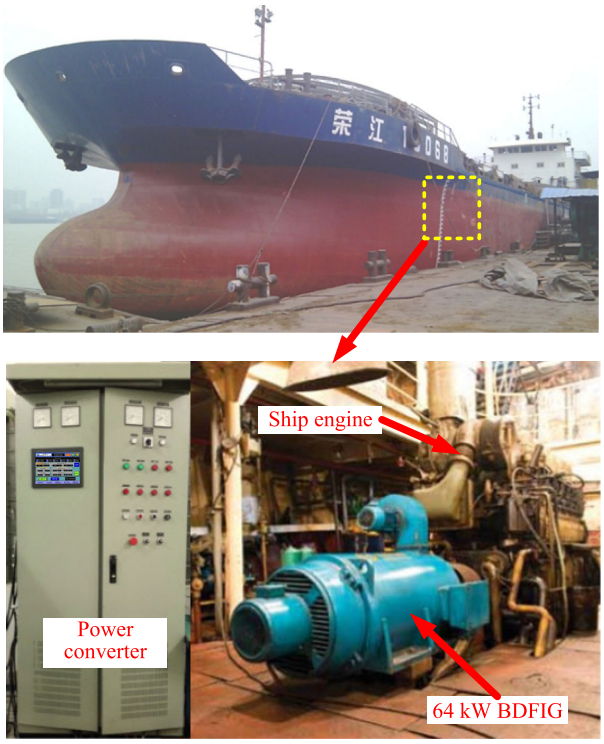

FIGURE 4. The BDFIG application in ship shaft power generation [12].

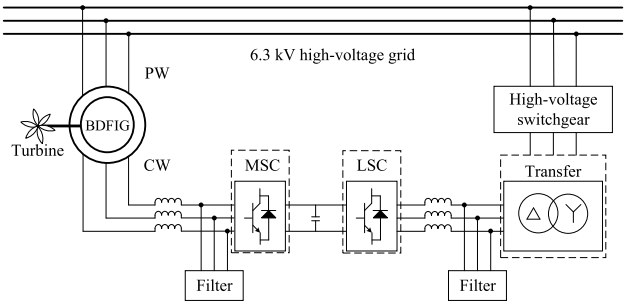

FIGURE 5. The BDFIG application in hydropower generation [16].

and differences between them through the classification and comparison. Since the cascade DFIG (CDFIG) has the same operation principle with the BDFIG, its control technologies will be also introduced in this paper. The rest of this paper is organized as follows. Sections II and III review the control technologies of BDFGs in grid-connected ac power generation under normal grid and faulty grids, respectively. In Sections IV and V, the progresses of BDFG control technologies for standalone ac power generation with normal loads and special loads are presented, respectively. The sensorless control technologies for BDFGs are introduced in Section VI. And, dc power generation control technologies are described in Section VII. Finally, Section VIII draws the conclusions and discusses the development trend in the future.

II. GRID-CONNECTED AC POWER GENERATION UNDER NORMAL GRID

BDFGs show commercial promise for grid-connected power generation systems, due to their lower operational costs and higher reliability as compared with DFIGs. Many control strategies have been developed for BDFGs over the years for grid-connected applications, among which the control strategies under normal grid can be summarized as follows.

A. VECTOR CONTROL

The most practical and preferred technique for BDFGs is the vector control (VC). The vector control methods of BDFG, in general, are derived from the dynamic mathematical models of BDFG based on different rotating reference frames. At present, the rotating reference frames used for BDFG mathematical modeling mainly includes: the single synchronous frame, the dual synchronous frames, and the slip-frequency rotating frame. Hence, the current vector control methods of BDFG can be divided into three categories, i.e., the single-synchronous-frame vector control (SSF-VC), the dual-synchronous-frame vector control (DSF-VC), and the slip-frequency-rotating-frame vector control (SFRF-VC).

1) SINGLE-SYNCHRONOUS-FRAME VECTOR CONTROL (SSF-VC)

According to the utilized synchronous frames, the SSF-VC methods can be divided into two main types, i.e., the VC methods based on the rotor synchronous frame and the ones based on the stator synchronous frame, as shown in TABLE 2.

TABLE 2. Classification of SSF-VC methods according to utilized synchronous frames.

Utilized synchronous frames	SSF-VC methods
Rotor synchronous frame	[17]-[21]
Stator synchronous frame	[22]-[35]

The rotor-flux-orientation VC methods have been developed in [17]–[19]. Although the control method proposed in [19] is for CDFIGs, it can be directly applied to BDFIG. A vector model under the rotor synchronous frame for the BDFIG-NLR has been established in [20]. Afterwards, based on the vector model developed in [20], a generalized VC strategy without rotor flux orientation has been proposed in [21], which only realizes the speed control, but does not achieve the adjustment of the reactive power. And, a hysteresis controller has been employed to regulate the CW current, which makes the CW current contain significant harmonics.

Based on the stator synchronous frame, quite a few SSF-VC methods have been proposed for different BDFGs as depicted in TABLE 3, which will be described in detail in the following paragraphs.

In [22], the BDFRG dynamic model under the single synchronous frame has been proposed, and a VC strategy based on the PW flux orientation has been developed, which realizes the decoupling control of torque and reactive power. In [23] and [24], the PW-flux-orientation and PW-voltage-orientation VC strategies for BDFRG have been proposed and compared. The difference between these two strategies is that the PW-flux-orientation VC strategies require

TABLE 3. Classification of SSF-VC methods based on the stator synchronous frame according to applicable machine types.

Applicable machine types	SSF-VC methods
BDFRG	[22]-[25]
CDFIG	[26]-[30]
BDFIG-NLR	[31]-[33]
BDFIG-WR	[34], [35]

the PW resistance to estimate the flux linkage, while the PW-voltage-orientation VC strategies can be implemented independently of machine parameters. However, the resulting problem is that the PW-voltage-orientation strategies is slightly worse than the PW-flux-orientation strategies in the response to reactive power. As the power rating of the BDFRG increases, the PW resistance would decrease, so that the performance difference between these two control strategies would also be smaller. In [25], a PW-voltage-orientation grid-synchronization strategy has been proposed for BDFRG to ensure that the PW voltage has the same phase-sequence, frequency and amplitude as the grid voltage. And, in this paper, two PW-voltage-orientation VC strategies have also been developed to achieve two different targets, i.e., unity power-factor operation and maximum electromagnetic torque per converter current.

A VC method based on the stator flux orientation of the power machine has been proposed for CDFIGs in [26]. It can basically realize the decoupling control of active and reactive power, although there is some cross coupling between the d- and q-axis control loops. Subsequently, the same authors as in [26] proposed a VC method based on the orientation of the virtual combined flux of the power machine and control machine stators in [27]. However, due to the serious cross coupling, the control method developed in [27] is not suitable for the decoupling control of active and reactive power, but it is feasible for the speed control. Another stator-flux-orientation VC method for CDFIGs has been proposed in [28] with a feedforward compensation for the decoupling of the stator current control loop of the control machine. The disadvantage of this method is that it requires the knowledge of the inductances of the power and the control machines, as well as the estimation of the stator and rotor fluxes of the power machine, which would degrade the system robustness under the mismatch of machine parameters. In [29] and [30], the other two stator-flux-orientation VC methods have also been investigated, which are with different feedforward compensation terms from the method in [28]. These feedforward compensation terms are also related to machine parameters, so that the system robustness against machine parameter variation would be deteriorated.

Ref. [31] proposed a vector model based on the unified reference frame for the BDFIG-NLR, in which both of the machine parameters and variables are referred to the PW side. Based on the model developed in [31], a VC strategy based on the PW flux orientation has been investigated in [32]. However, it additionally introduces a PW current control loop, which makes the control parameter tuning complicated. According to the vector model proposed in [31], the more concise PW-flux-orientation VC strategy has been studied in [33], which removes the CW current loop and can directly control the reactive power and speed by regulating the d- and q-axis voltages of CW, respectively. The potential problem of this method is that the CW is with the risk of transient overcurrent when the speed and reactive power commands change rapidly due to the CW current being not controlled.

For the BDFIG-WR, the grid-flux-orientation VC strategy has been proposed to implement the decoupling control of active and reactive power with feedforward compensation [34]. Different from the grid voltage orientation, the grid flux orientation is achieved by q-axis of the synchronous frame being aligned with the grid voltage vector. Besides, the PW-flux-orientation VC strategy for the wound-rotor BDFIG has also been investigated in [35], which is without any feedforward compensation terms at all.

The frame orientation style is a key element for VC methods. Based on the above analysis, the SSF-VC methods can be classified into six main categories according to frame orientation styles, as depicted in TABLE 4. From TABLE 4, it can be seen that most of the research works focus on the PW-flux-orientation VC methods for BDFGs and the VC methods based on stator winding flux orientation of the power machine for the CDFIG. The main reason is that the VC methods based on the flux orientation of PW or power machine stator winding can better achieve the decoupling of active power and reactive power.

TABLE 4. Classification of SSF-VC methods according to frame orientation styles.

Frame orientation styles	SSF-VC methods
Rotor flux orientation	[17]-[19]
PW (Power machine stator winding) flux orientation	[22]-[24], [26], [28]-[33], [35]
Virtual combined flux orientation	[27]
PW voltage orientation	[23]-[25]
Grid flux orientation	[34]
Without orientation	[20], [21]

2) DUAL-SYNCHRONOUS-FRAME VECTOR CONTROL (DSF-VC)

The BDFG can be regarded as the combination of PW and CW subsystems, and the BDFG dynamic model in the dual synchronous frames has been established in [36]. The dual synchronous frames contain the PW subsystem synchronous frame and the CW subsystem synchronous frame. A few DSF-VC methods have been proposed for BDFIG [37], [38] and BDFRG [39], [40].

In [37] and [38], the rotor flux orientation of BDFIG is carried out in both PW and CW subsystems, so that the input and output quantities of the two subsystems in the steady state are no longer time-variable but constant. Consequently, the

CW flux can be controlled by the d-axis CW current, and the electromagnetic torque can be controlled by the q-axis CW current. However, in comparison with the SSF-VC methods, the DSF-VC methods is more complicated in the estimation of the electromagnetic torque. The reason is that the d- and q-axis CW currents should be transformed to the PW subsystem according to the angle difference between the two synchronous frames when calculating the electromagnetic torque.

The dynamic model of BDFRG is simpler than that of BDFIG, since there are no voltage and flux equations in the dynamic model of BDFRG. In [39], the dynamic model of BDFRG has been expressed in two separate reference frames, which makes the model of BDFRG very similar to that of the double-excited slip ring induction machine (DESRIM). Consequently, the existing control methods for DESRIM can be essentially applied to BDFRG, although the operating principles of the two machines are fundamentally different. In [40], based on the dual-synchronous-frame dynamic model, a multiple-input multiple-output (MIMO) robust controller has been proposed for the BDFRG-based wind energy conversion system. The MIMO controller can achieve two objectives at the same time, i.e., the wind energy conversion maximization and the machine copper losses minimization.

3) SLIP-FREQUENCY-ROTATING-FRAME VECTOR CONTROL (SFRF-VC)

In general, the PW is established on the stationary frame $A_1B_1C_1$. Through the magnetic coupling of the rotor, the CW current can induce an air gap magnetic field with the same frequency as the PW current. As a result, the angular frequency of the CW current vector relative to the frame $A_1B_1C_1$ can be regarded as the PW current frequency ω_1. Since the actual frequency of the CW current is ω_2, a CW frame $A_2B_2C_2$ rotating at the slip frequency (ω_1-ω_2) can be constructed, in which the angular frequency of the CW current vector is still ω_2, as shown in Fig. 6(a) [41]. Based on the constructed frames $A_1B_1C_1$ and $A_2B_2C_2$, the BDFRG mathematical model similar to DFIG has been established, and the corresponding control strategy has been proposed in [41] and [42]. The proposed control strategy employs only the CW current for magnetic excitation, while the PW current is used entirely to generate electromagnetic torque, as shown in Fig. 6(b). Consequently, the greater dynamic electromagnetic torque can be provided, and the dynamic response of system can be significantly improved.

B. DIRECT CONTROL

1) DIRECT POWER CONTROL

The direct power control (DPC) can directly decouple and separately control the active and reactive power of BDFGs. The DPC requires less computation and does not need to observe the PW flux amplitude, which can well address the issue of the poor real-time performance caused by the flux observer being sensitive to BDFG parameter variations. The DPC has been proposed for CDFIGs in [43] as an alternative to the VC scheme of CDFIGs. Such strategy has fast dynamic response, simple implementation and robustness. The DPC provides direct regulation of the machine power by selecting proper voltage vectors from the lookup-tables. However, the converter switching frequency varies with operating conditions, which results in large power ripple and current distortion.

To improve such shortcomings, while keeping the advantages of DPC over the VC, a super-twisting sliding mode direct power control (SSM-DPC) strategy has been proposed in [44] for the BDFIGs, as given in Fig. 7. The SSM-DPC strategy can control active and reactive power directly without the need of phase locked loop. Moreover, its transient performance is similar to the conventional DPC and its steady-state performance is the same as the vector control. The proposed controller in [44] is robust to uncertainties toward parameter variations and achieves the constant converter switching frequency by using space vector modulation.

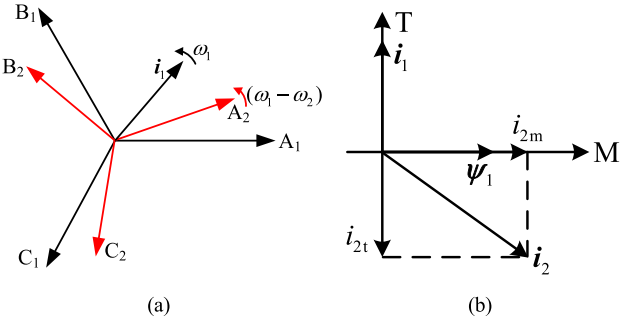

FIGURE 6. The SFRF-VC method. (a) Structure of SFRF. (b) The obtained PW and CW current vectors by the SFRF-VC method proposed in [41] and [42].

In [45], the DPC based on the twelve sections has been adopted to implement the power tracking of the open-winding BDFIG system as illustrated in Fig. 5. In comparison with the typical BDFIG DPC system based on the six and twelve sections, the advantages of the proposed scheme lie in lower converter capacity and cost, simpler control structure, more flexible control mode, and better operation performance and fault-tolerant ability.

2) DIRECT TORQUE CONTROL

Direct torque control (DTC) has features of simple structure, fast dynamic-response torque, good robustness and low-reliability on machine parameters, which solve the problems about complicated structure, large amount of calculation and sensitive to parameter change of vector control [46]-[53]. For the traditional DTC, hysteresis comparator cannot distinguish the size of torque and flux linkage error. Controller applies voltage vector to the whole control cycle. In the cycle with smaller torque error, the voltage makes the torque to achieve a given value quickly in a short time, and unchanged switch state of inverter makes torque along the original direction, then huge torque ripple occurred.

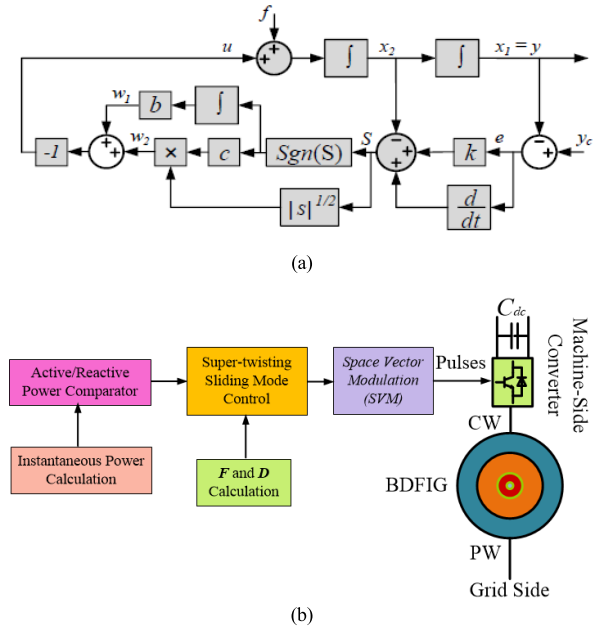

FIGURE 7. Structure of the proposed SSM-DPC strategy for BDFIG [44]. (a) Schematic diagram of the super-twisting sliding mode control. (b) Overall DPC strategy with the super-twisting sliding mode control, where *F* and *D* are two matrices determined the time-derivative formula of sliding surface.

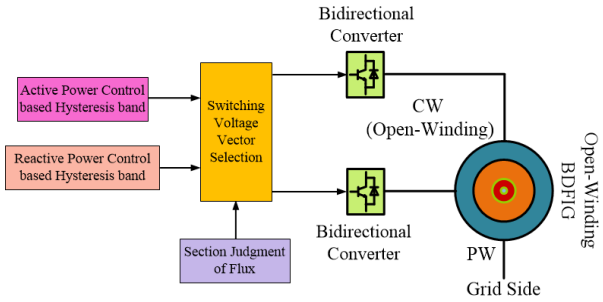

FIGURE 8. DPC diagram of the open-winding BDFIG [45].

To reject the torque ripple in DTC, scholars from all over the world did a lot of research and put forward many improvement methods, such as using the voltage space vector modulation (SVM–DTC) [47], the discrete space voltage vector [48], fuzzy control [49], [50], predictive control [51], duty ratio modulation [52], combination of predictive control and duty ratio modulation [53].

The SVM–DTC algorithm in [47] can effectively reduce the torque ripple but requires a large amount of calculation and more parameters. The discrete space vector modulation (DSVM) in [48] has the advantage of good robustness in direct vector control, but the improvement of control accuracy is based on the premise of breakdown voltage vector which increased the complexity of the control system.

In [49], a fuzzy control algorithm with a good dynamic performance is presented, which can effectively reduce the torque ripple. But in the state machine, variable membership has uncertainty; if membership choice is not appropriate, the system performance will be deteriorated. In [50], the improved fuzzy DSVM–DTC control method is used to strengthen the control of torque and speed, but the control rules are very complex due to the fuzzy controller being with five inputs. The torque prediction is used in [51], which reduces torque ripple and improves the waveform of stator current, but needs a little huge computation.

In [52], the DTC method based on duty ratio modulation is studied, in which the non-zero voltage vector only acts partial time in one control cycle and zero voltage vector acts on the rest time. In [53], a method of combining predictive control and duty ratio modulation has been proposed, as given in Fig. 9, to reduce the torque ripple. This control method can reduce the torque ripple and can keep the advantages of fast torque response and simple control of the traditional DTC.

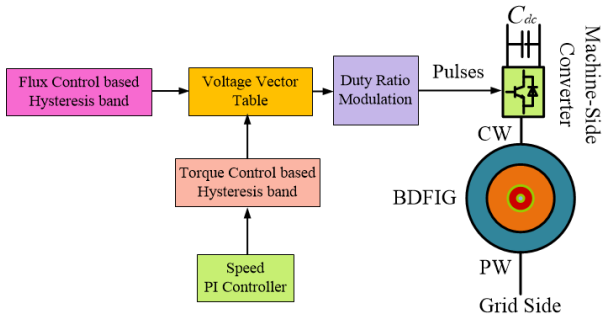

FIGURE 9. The block diagram of the duty ratio modulation DTC for BDFIG proposed in [53].

C. INDIRECT CONTROL

The indirect stator-quantities control (ISC) is a new control strategy for BDFIG [54]–[56]. Compared to VC and DTC control schemes, there are some remarkable advantages to the ISC, such as not requiring rotating coordinate transformations and flux linkage orientation, less sensitivity to machine parameters, simpler system structure and the capability of current-limit.

In [55], the control structure of the ISC strategy has been demonstrated by means of theoretical derivation as well as experimental results. The dynamic performance of the ISC controller has been tested over wide range of speeds from sub-synchronous to super-synchronous, and also under the conditions of sudden load change.

The study in [56] has further developed the dynamic control of reactive power for the BDFIG with the ISC scheme shown in Fig. 10. Detailed theoretical analysis has been done to show the controller structure of the reactive power. As a result, both speed and the reactive power can be controlled simultaneously. These control features are achieved in a static reference frame, and rotating coordinate transformations and flux linkage orientation are unnecessary, so the ISC is simpler to implement in practice.

III. GRID-CONNECTED AC POWER GENERATION UNDER FAULTY GRIDS

A. UNBALANCED-GRID RIDE-THROUGH (UGRT)

A few literatures have studied the operation of BDFIG under unbalanced grid conditions [43], [57]–[59]. When the grid is

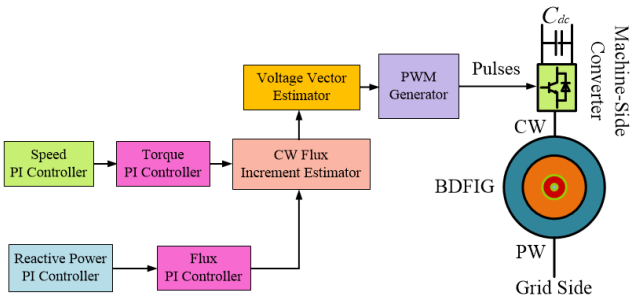

FIGURE 10. Block diagram of the proposed indirect stator-quantities control system with reactive power controller in [56].

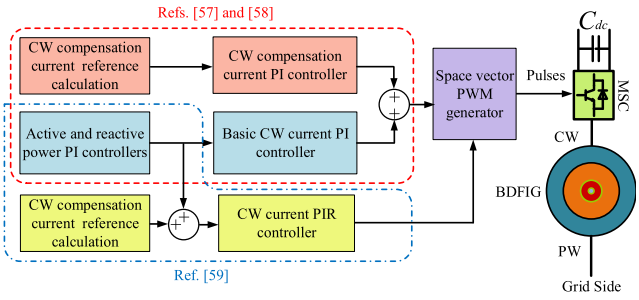

FIGURE 11. Summarized control structures presented in [57]–[59] for UGRT with PI/PIR controllers, respectively.

unbalanced, the PW current is unbalanced, torque and power will oscillate at twice the PW frequency and hence, the CW current is also distorted.

In [43], the active and reactive power compensation terms are added to the reference values of active and reactive power, and then the DPC strategy is employed to control the power with eliminating the negative-sequence components of the power machine stator currents.

Different from the work in [43] based on DPC, all the studies in [57]–[59] based on the VC method can be summarized in Fig. 11. The study in [57] has proposed the dual proportional-integral (PI) vector control, regulating the positive-sequence CW current controller for active and reactive power generation, and the negative-sequence CW current controller for three different control targets. The process of voltage and current decomposition not only made the model and algorithm complex, but also introduced delay by band-trap filters. The control scheme proposed in [58] is with the similar structure as that in [57], although it is based on the dual synchronous rotating frames. In [59], an improved VC has been proposed for the BDFIG under unbalanced grid conditions by introducing proportional-integral-resonant (PIR) controller in single synchronous reference frame. Compared to the existed solutions, the algorithm as proposed in [59] is easy to implement, fast in transient response performance, and also robust under parameter variations. Furthermore, no negative-sequence voltage and current decomposition is required in [59], which would simplify the algorithm and provide fast dynamic response.

It can be noted that the BDFIG torque ripple caused by the unbalanced grid has not attracted enough attention, as few papers have discussed this topic expect [59]. However, the torque ripple should be the most concerned issue in wind power system for its degradation in gear box and reduction of life span. Hence, more studies on the UGRT of BDFIGs are greatly desirable in the future.

B. LVRT

The LVRT capability indicates that grid-connected wind turbines must remain connected and supply reactive current to the grid during grid voltage dips. The LVRT is the most important indicator in many national grid codes [60]–[67].

The LVRT methods can be divided into two categories, i.e., based on the hardware and based on the software, as shown in Fig. 12. The hardware mainly includes the crowbar and series dynamic resistor (SDR). The use of a crowbar or SDR enables the BDFIG to ride through the most serious voltage dips, However, some unavoidable problems are caused by these hardware devices, such as increasing system cost and reactive power consumption [60]–[62].

The software-based methods, i.e. the crowbarless LVRT control methods, can be implemented in the rotating frame and the static frame. To date, the crowbarless LVRT control schemes for BDFIGs developed in [63]–[67] are all essentially implemented in the rotating reference frame.

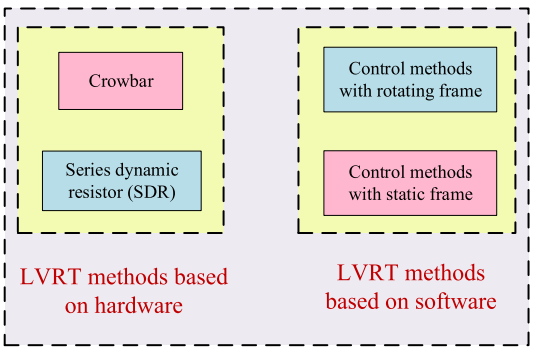

FIGURE 12. Different kinds of LVRT methods for the grid-connected BDFIG systems [63]–[67].

The control strategies proposed in [63] and [64] can compensate for the couplings between the two axes of the CW current, with different compensation terms. The simulation results in [63] and [64] show that the BDFIG cannot ride through severe low-voltage dips with the proposed control strategies. In [65], a crowbarless control strategy has been proposed to enable the ride-through of the BDFIG under the 100% symmetrical grid voltage dip, and only the forward sequence has been controlled in the LVRT mode. However, under the 100% symmetrical grid voltage dip, there is still a zero-sequence component in the PW flux linkage. The ignorance of the zero-sequence component may result in unsatisfactory LVRT behavior. In [66], the authors have presented a simple control strategy for riding through asymmetrical faults. The experimental results in [65] and [66] indicate that when the BDFIG rotor speed is 96% of the maximum rotor speed (100% is the most severe), the CW current peak is

approximately 2.42 p.u. of the BDFIG CW current rating or 2 p.u. of the transient IGBT current rating. As can be seen from these experimental results, the LVRT performance got by the hardware-based methods in [65] and [66] is a bit worse that that obtained by the software-based method in [60]. In [67], in order to achieve LVRT under symmetrical grid voltage dips, the integral part of the CW current PI controller is removed and the proportional gain is optimized in the LVRT mode, so that the order of the control system can be reduced and the d- and q-axis currents of CW and PW can quickly converge. Consequently, the overcurrent and oscillation of the CW and PW currents can be avoided during symmetrical grid voltage dips.

In [68], a crowbarless LVRT control strategy has been proposed in the static reference frame, which is based on the flux linkage tracking under symmetrical voltage dips, as shown in Fig. 13. To both suppress the CW current and increase PW reactive current, a time-sharing control and CW current-first control solution have been proposed. In the most severe case, where the BDFIG rotor speed is 100% of the maximum rotor speed and under 100% symmetrical voltage dips, the experimental results have shown that the CW current peak could be limited to 2 p.u. of the CW current rating and the torque ripple be small during the fault.

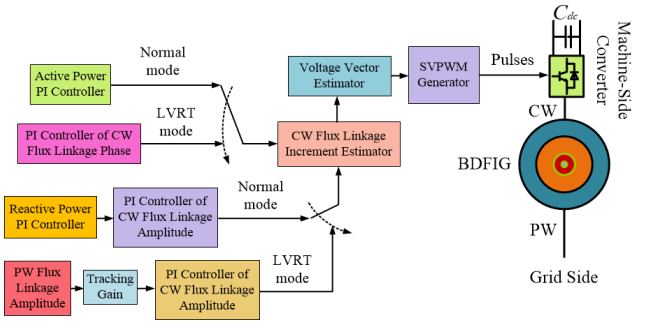

FIGURE 13. Block diagram of the crowbarless LVRT control strategy based on flux linkage tracking for BDFIG under symmetrical voltage dips proposed in [68].

IV. STANDALONE AC POWER GENERATION WITH NORMAL LOADS

The key control loop for the standalone ac BDFG power generation system is the CW current control loop. The currently proposed CW current controllers can be divided into three main categories, i.e., PI controllers without decoupling, PI controllers with decoupling, and predictive controllers.

A. PI CONTROLLERS FOR CW CURRENT WITHOUT DECOUPLING

The relationship between CW current and CW voltage can be expressed as [12]

$$i_{2d} = (R_2 + \sigma_2 L_2 s)u_{2d} + \underbrace{(\alpha_1 i_{2q} + \alpha_2 i_{1d} + \alpha_3 i_{1q})}_{\text{Cross-coupling disturbance}} \quad (1)$$

$$i_{2q} = (R_2 + \sigma_2 L_2 s)u_{2q} + \underbrace{(\alpha_4 i_{2d} + \alpha_5 i_{1d} + \alpha_6 i_{1q})}_{\text{Cross-coupling disturbance}} \quad (2)$$

where $\sigma_2 = 1 - L_{2r}^2/(L_2 L_r)$ is the leakage constant of the CW, the coefficients α_1, α_2, α_3, α_4, α_5 and α_6 are related to machine parameters, PW frequency and rotor speed.

From (1) and (2), ignoring the cross-coupling disturbance, the structure of the CW current controller can be designed as a proportional-integral (PI) control loop shown in Fig. 14.

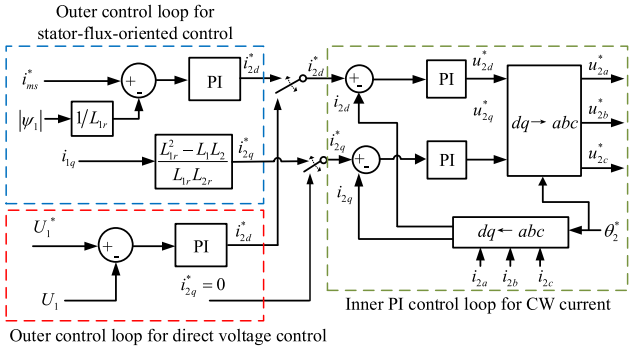

FIGURE 14. The stator-flux-oriented control and the direct voltage control based on CW current PI controller without decoupling [69], [12].

Both of the stator-flux-oriented control proposed in [69] and the direct voltage control proposed in [12] are based on the inner PI control loop for CW current shown in Fig. 14. The difference between the stator-flux-oriented control and the direct voltage control is the outer control loop. In the stator-flux-oriented control, the PW voltage is indirectly regulated by adjusting the equivalent PW magnetizing current in the outer control loop, and the PW flux orientation is achieved by regulating the q-axis CW current proportional to the q-axis PW current. Consequently, the feedback value of the equivalent PW magnetizing current and the reference value of the q-axis CW current depend on machine parameters, such as the mutual- and self- inductances, which would degrade the robustness of the control system. In order to address this issue, the direct voltage control is proposed, where the outer control loop is used to adjust the amplitude of PW voltage directly. And, the reference value of the q-axis CW current in the direct voltage control is set to zero, which means that the direct voltage control method is based on the CW current orientation.

In [12], the CW current control loop shown in Fig. 14 has been tested on a 60-kVA BDFIG with the natural synchronous speed of 500 rpm. The test is carried out at the sub- and super-synchronous speeds, respectively. The reference value of the d-axis CW current is around 15% of the rated current, and that of the q-axis CW current is zero. From the simulated and experimental results shown in Fig. 15, it can be seen that the settling time of CW current is 50 and 70 ms at the sub- and super-synchronous speeds, respectively, with the d-axis CW current overshoot of around 7.5%.

However, it is difficult to obtain a fast response speed for CW current with small overshoot based on the control method shown in Fig. 14. The main reason for this problem is that

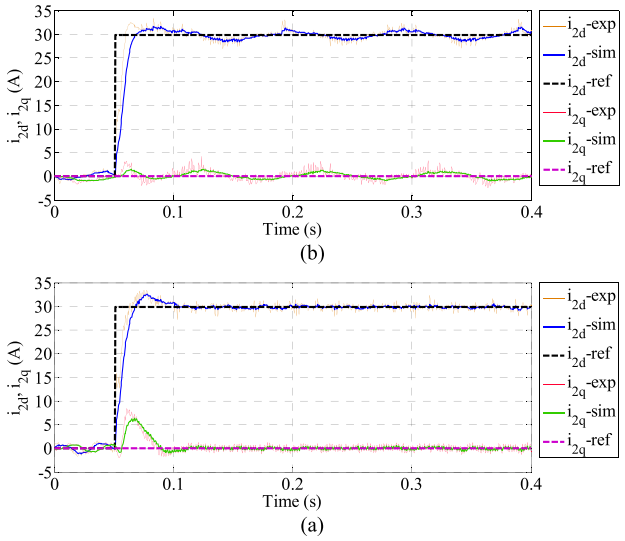

FIGURE 15. Simulated and experimental results of the CW current control loop shown in Fig. 14 [12]. (a) At the sub-synchronous speed of 400 rpm. (b) At the super-synchronous speed of 600 rpm.

the d- and q-axis control channels of the CW current loop is severely coupled as shown in (1) and (2), which cannot be ignored for obtaining fast response.

B. PI CONTROLLERS FOR CW CURRENT WITH DECOUPLING

In order to improve the dynamic performance of the CW current controller, the CW current control loop with cross feedforward compensation is proposed in [70], as shown in Fig. 16. Besides, the d- and q-axis PW currents are also the inputs of the feedforward compensation terms, which can get further benefits from the proposed feedforward compensation method, i.e., suppression over load disturbances, and so on.

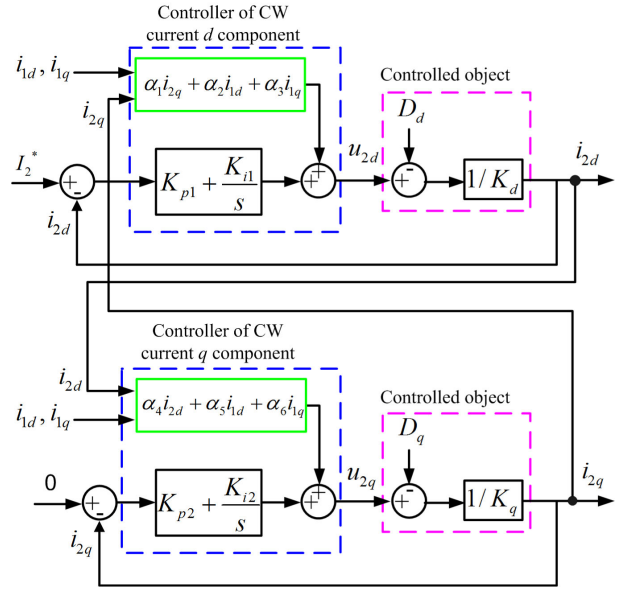

FIGURE 16. The CW current control loop with cross feedforward compensation proposed in [70].

The CW current control loop with cross feedforward compensation proposed in [70] has been tested on a 30 kVA BDFIG under the sub-synchronous speed of 600 rpm and the super-synchronous speed of 1200 rpm, respectively. Similar to the test shown in Fig. 15, the reference value of the d-axis CW current is also around 15% of the rated current, and that of the q-axis CW current is zero. As can be seen from Fig. 17, with cross feedforward compensation, the settling time of CW current can be reduced to 26 and 38 ms under the similar overshoot of d-axis CW current (around 7.5%) at the sub- and super-synchronous speeds, respectively. Hence, the control method proposed in [70] can significantly enhance the dynamic performance of the CW current control loop in comparison with that proposed in [12]. Also, the similar feedforward compensation method has been proposed in [71].

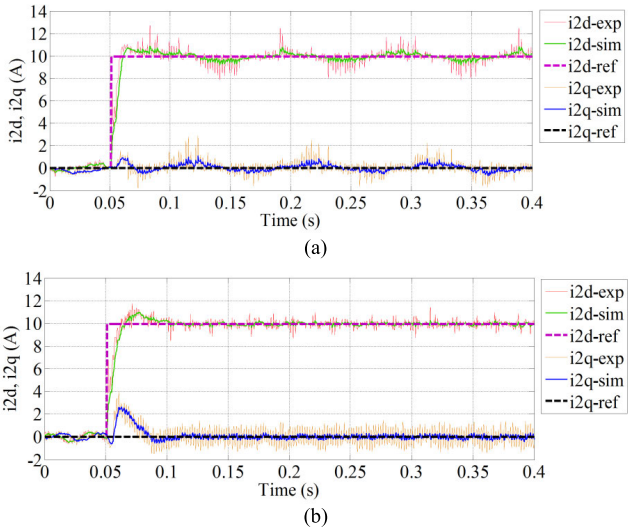

FIGURE 17. Simulated and experimental results of the CW current control loop shown in Fig. 16 [70]. (a) At the sub-synchronous speed of 600 rpm. (b) At the super-synchronous speed of 1200 rpm.

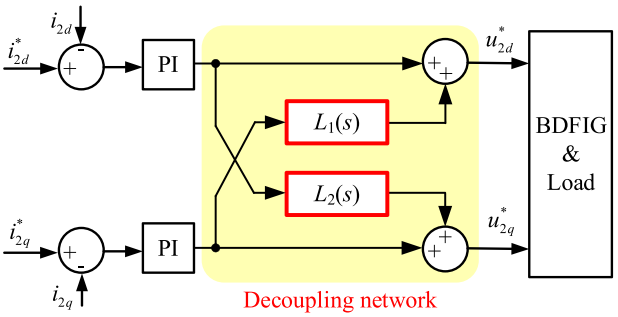

FIGURE 18. The CW current control loop with decoupling network proposed in [72].

Besides, in [72], a decoupling network is developed to eliminate the influence of the cross-coupling disturbance in the CW current control loop, as shown in Fig. 18. The models of the BDFIG and the load are integrated to a dual-input-dual-output system, in which the inputs are u_{2d} and u_{2q}, and the outputs are i_{2d} and i_{2q}. And then, by selecting appropriate

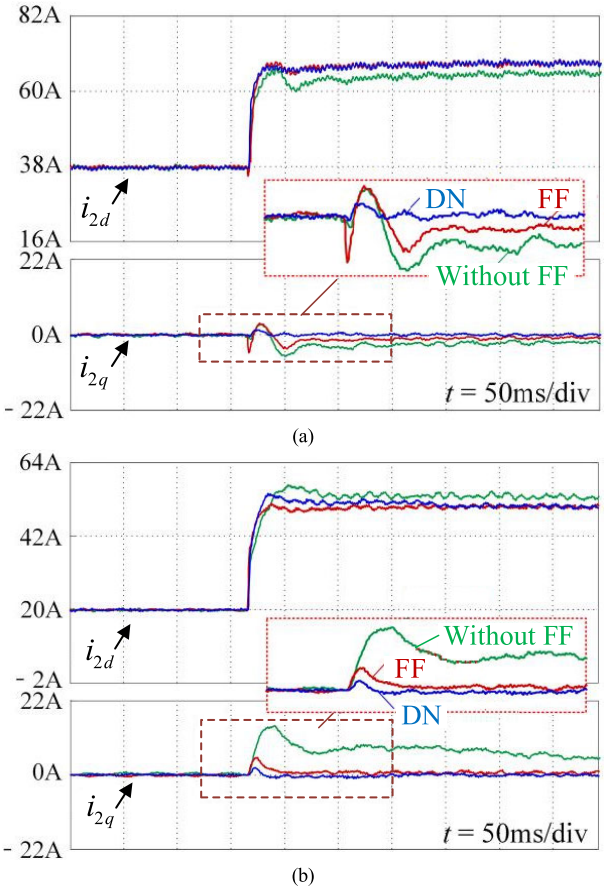

FIGURE 19. Experimental results of the CW current control loop shown in Fig. 12, where DN and FF indicate decoupling network and feedforward, respectively. (t = 50ms/div). (a) At the sub-synchronous speed of 350 rpm. (b) At the super-synchronous speed of 650 rpm.

transfer functions $L_1(s)$ and $L_2(s)$, the d- and q-axis control channels of the CW current loop can be completely decoupled. In general, $L_1(s)$ and $L_2(s)$ can be designed as the fifth-order transfer functions.

The control method proposed in in [72] has been verified on a 32 kW BDFIG with the natural synchronous speed of 500 rpm, in comparison with the feedforward compensation method proposed in [71] and the method without feedforward compensation. From some of typical experimental results depicted in Fig. 19, it can be seen that the CW current control loop with the decoupling network possesses the best dynamic performance among the three methods. However, the dependence of the decoupling network design on the load model may make this method difficult for industrial applications.

C. PREDICTIVE CONTROLLERS FOR CW CURRENT

In order to improve current tracking accuracy, the model predictive current control (MPCC) method has been developed for standalone BDFIG [73]. The predicted CW current expressions can be expressed as

$$i_{2d}(k+1) = \left(1-\frac{R_2}{\sigma_2}T_s\right) i_{2d}(k) + \frac{T_s}{\sigma_2}U_{2d}(k) - \frac{T_s}{\sigma_2}D_{2d} \quad (3)$$

$$i_{2q}(k+1) = \left[1 - \frac{R_2 + \frac{R_r L_{2r}^2 \omega_1}{L_r^2(\omega_1 - p_2\omega_r)}}{\sigma_2} T_s\right] i_{2q}(k) + \frac{T_s}{\sigma_2}U_{2q}(k) - \frac{T_s}{\sigma_2}D_{2q} \quad (4)$$

where $\sigma_2 = L_2 - L_{2r}^2/L_r$, T_s is the sampling time, and D_{2d} and D_{2q} are the cross-coupling disturbance between d- and q-axis current.

Since the MPCC is designed to enhance the current tracking accuracy, the cost function of MPCC can be expressed as

$$g = [i_{2dref} - i_{2d}(k+1)]^2 + [i_{2qref} - i_{2q}(k+1)]^2. \quad (5)$$

However, as can be seen from (3) and (4), the MPCC method heavily depends on machine parameters. When the BDFIG temperature rises or magnetic saturation occurs, the machine parameters will change, which would degrade the performance of the MPCC.

In order to address this issue, the nonparametric predictive current control (NPCC) method for standalone BDFIG is proposed in [74]. With NPCC, the predicted currents at the $(k+2)$th instant with delay compensation can be derived as

$$i_{2d}(k+2) = i_{2d}(k) + X_{2d}U_{2d}(k) + X_{2d}U_{2d}(k+1) + 2[\Delta i_{2d}(k-1) - X_{2d}U_{2d}(k-1)] \quad (6)$$

$$i_{2q}(k+2) = i_{2q}(k) + X_{2q}U_{2q}(k) + X_{2q}U_{2q}(k+1) + 2[\Delta i_{2q}(k-1) - X_{2q}U_{2q}(k-1)] \quad (7)$$

where

$$X_{2d} = \frac{\Delta i_{2d}(k-1) - \Delta i_{2d}(k-2)}{U_{2d}(k-1) - U_{2d}(k-2)},$$
$$X_{2q} = \frac{\Delta i_{2q}(k-1) - \Delta i_{2q}(k-2)}{U_{2q}(k-1) - U_{2q}(k-2)}.$$

Actually, the coefficients X_{2d} and X_{2q} can approximately represent the parameter (T_s/σ_2), which frequently appears in the current prediction expressions of MPCC. In other words, the NPCC can use the sampled BDFIG signals rather than machine parameters to predict the future current. Besides, the cost function of NPCC is the same as that of MPCC.

Simulation of MPCC and NPCC is carried out on a 30-kVA BDFIG under the sub-synchronous speed of 600 rpm, whose results are shown in Fig. 20 and Fig. 21 [74]. The inductances of PW and CW are changed from 100% to 80% at 0.4 s, respectively. With MPCC, a significant steady-state error in the d-axis CW current is generated by the varying PW and CW inductances. Fortunately, the NPCC can avoid this problem under the same operation condition.

V. STANDALONE AC POWER GENERATION WITH SPECIAL LOADS

Generally, standalone generation systems are susceptible to special loads, e.g., unbalanced loads and nonlinear loads. The unbalanced loads would generate negative-sequence PW

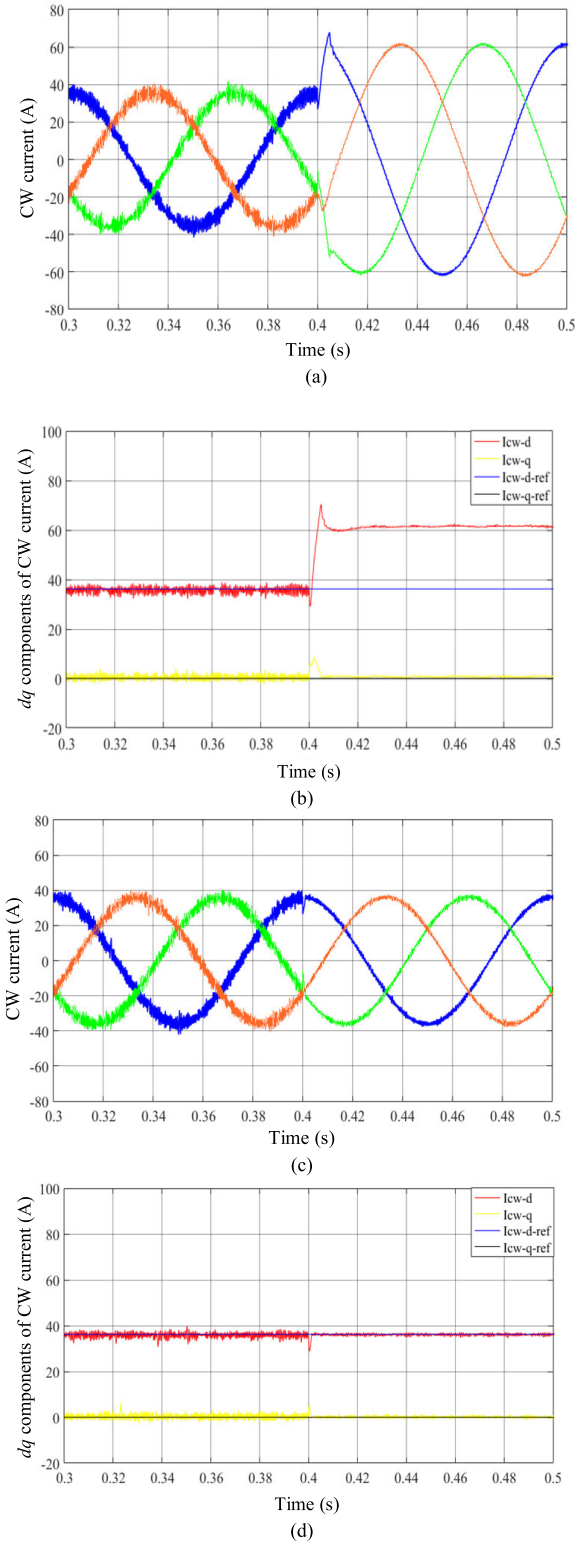

FIGURE 20. Simulation results of MPCC and NPCC with the PW inductance change from 100% to 80% [74]. (a) CW three-phase current with MPCC. (b) *d*- and *q*-axis components of CW current with MPCC. (c) CW three-phase current with NPCC. (d) *d*- and *q*-axis components of CW current with NPCC.

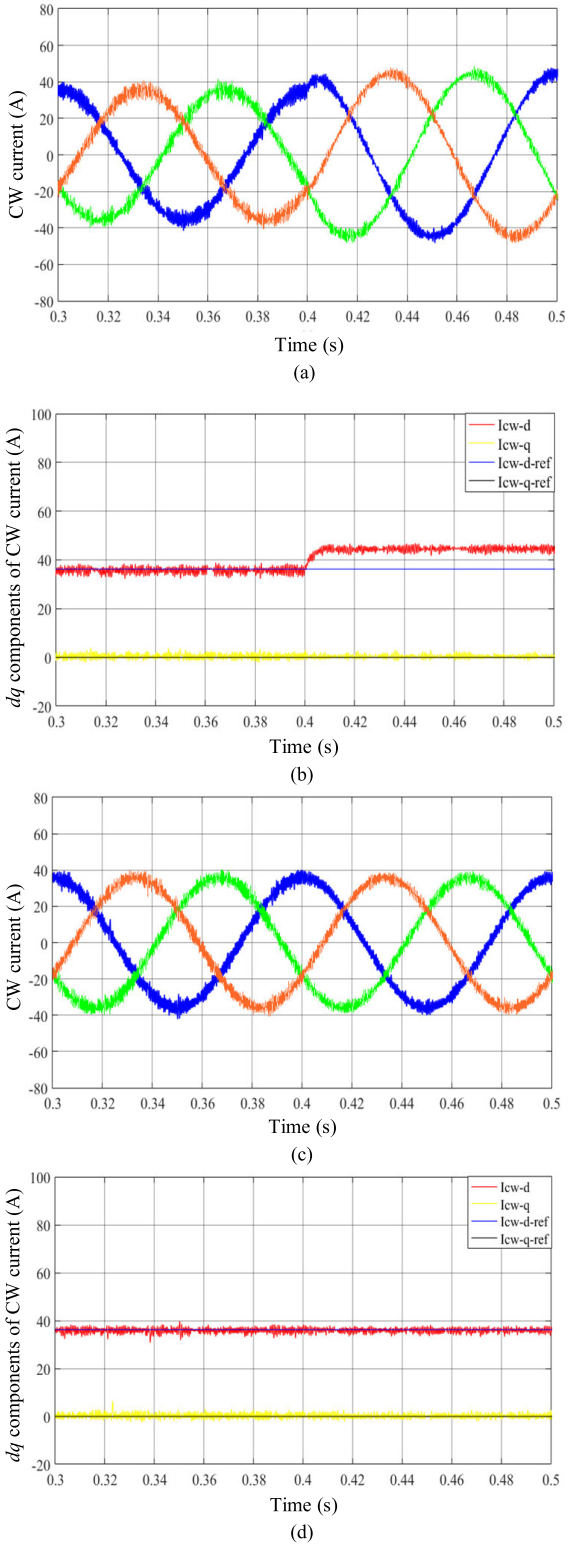

FIGURE 21. Simulation results of MPCC and NPCC with the CW inductance change from 100% to 80% [74]. (a) CW three-phase current with MPCC. (b) *d*- and *q*-axis CW current with MPCC. (c) CW three-phase current with NPCC. (d) *d*- and *q*-axis CW current with NPCC.

voltage, and the nonlinear loads can introduce low-order harmonic voltages into PW. These control strategies mentioned above do not take into account the stable operation under these special loads. To solve this problem, some compensation methods have been developed, which can be divided into two main categories, i.e., the compensation methods based on

the single power converter and those based on the dual power converters.

A. COMPENSATION BASED ON SINGLE POWER CONVERTER

The voltage at the PCC of the standalone BDFIG system can be expressed as

$$\begin{aligned} u_{\mathrm{PCC}} &= E_1 - R_1 i_1 - L_1 s i_1 \\ &= E_1 - \underbrace{(R_1 i_{1f} + L_1 s i_{1f})}_{\text{Fundamental voltage drop}} \underbrace{-(R_1 \sum i_{1h} + L_1 \sum s i_{1h})}_{\text{Harmonic voltage drop}} \end{aligned} \tag{8}$$

where E_1 is the inductive electromotive force (EMF) of PW, i_{1f} the PW fundamental current, and i_{1h} the negative-sequence and harmonic currents.

As can be seen from (8), the negative-sequence and hormonic components of the PW voltage can be eliminated by producing an additional compensation EMF E_{1h} to compensate the harmonic voltage drop in the PW. The E_{1h} can be obtained by MSC injecting compensation current to CW. Also, the negative-sequence and hormonic components of PW voltage can be suppressed by removing the negative-sequence and harmonic currents i_{1h}, which can be achieved by LSC injecting compensation current to unbalanced and nonlinear loads. Hence, the compensation methods based on the single power converter can be classified as two types, i.e., the method based on MSC and the one based on LSC.

According the calculation mode of CW voltage compensation components, the compensation methods based on MSC can be divided into two main categories, as illustrated in Fig. 22. Fig. 22(a) and (b) present the compensation method with indirect calculation of CW voltage compensation components, and Fig. 22(c) shows the one with direct calculation of CW voltage compensation components.

In Fig. 22(a), both the obtained CW current compensation components and the basic CW current reference are in the same rotating frame, so that the fundamental and compensation components of CW voltage can be calculated at the same time. The control schemes proposed in [75] and [76] can be classified into the control method shown in Fig. 22(a). A negative-sequence voltage compensation scheme for unbalanced standalone BDFIGs has been proposed in [75], which is implemented in the machine side converter (MSC). The negative-sequence PW voltage is extract by the dual second-order generalized integrators (DSOGI) and then regulated by the PI controller to obtain the compensation current of CW. Consequently, the reference value of the CW current in the positive-sequence frame is with both the dc and ac components, which causes that the PIR controllers must be utilized in the CW current control loop. Another control scheme based the similar control concept has also been developed in [76], which can handle both the unbalanced and nonlinear loads. The multiple second-order generalized integrators (MSOGI) is adopted to obtain the negative-sequence and 5th and 7th harmonic components of

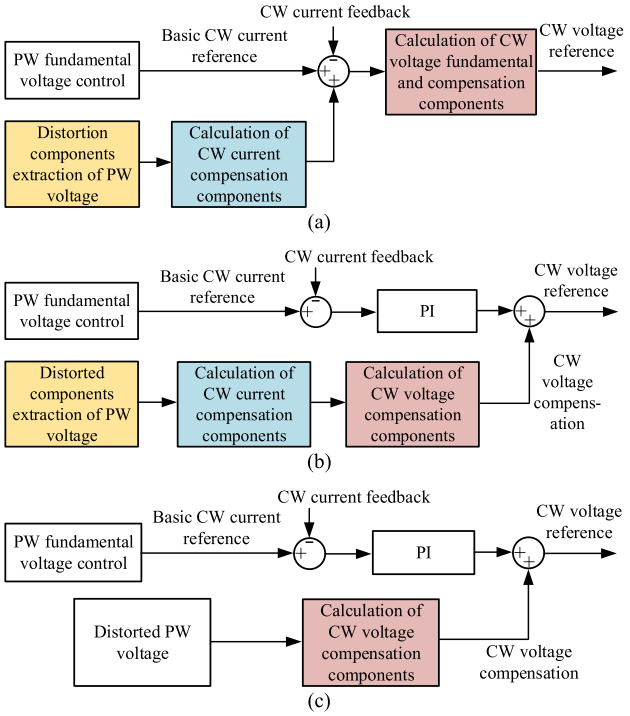

FIGURE 22. Different compensation methods based on MSC for standalone BDFIG under special loads. (a) Indirect calculation of CW voltage compensation components-Type I. (b) Indirect calculation of CW voltage compensation components-Type II. (c) Direct calculation of CW voltage compensation components.

PW voltage, and the dual frequency resonance (DFR) controller has to be employed in the CW current control loop.

The control structure shown in Fig. 22(b) is a little different from that shown in Fig. 22(a). In Fig. 22(b), the CW voltage fundamental component and the compensation components are obtained separately, and the latter ones have to be transformed to the fundamental frame. The negative-sequence voltage compensation scheme proposed in [77] belongs to the method depicted in Fig. 22(b). In [77], the amplitudes of the positive-and negative-sequence PW voltages can be regulated separately with a robust rotor speed observer.

The common feature of the compensation methods shown in Fig. 22(a) and (b) is that the CW current compensation components have to be obtained before calculating the CW voltage compensation components. Therefore, in essence, the two compensation methods are the same. However, the indirect obtaining of CW voltage compensation components results that too many PI or resonant controllers have to be employed, which causes that the control algorithm is too complicated for actual industry applications.

In order to address this issue, the compensation method shown in Fig. 22(c) is developed, which employs only one compensator to calculate the CW voltage compensation components directly. Hence, it can be significantly simplified in comparison to the methods depicted in Fig. 22(a) and (b). A typical case of the method shown in Fig. 22(c) has been introduced in [78], where an improved control strategy based on the dual-resonant controller (DRC) is proposed to minimize

both the unbalance and nonlinear effects of PW voltage at the same time. The CW current controller is just a simple PI controller. The DRC composes of two parts: unbalance resonant controller with the resonant frequency of 2-times PW frequency and the harmonics resonant controller with the resonant frequency of 6-times PW frequency. The unbalance resonant controller is used to compensate the unbalanced and 3rd harmonic components in the PW voltage. And, the harmonics resonant controller is adopted to eliminate the 5th and 7th harmonics of PW voltage. It is not necessary to extract the negative-sequence and harmonic components of PW voltage.

The compensation method based on LSC for standalone BDFIG under special loads can be briefly described as Fig. 23. It utilizes LSC to inject compensation current to unbalanced and nonlinear loads, so that the negative-sequence and hormonic components of the loads can be no longer supplied by PW. Ref. [79] employs this method to successfully eliminate the harmonic voltages of PW caused by nonlinear loads. Generally, when using this kind of compensation method, the distorted components of PW voltage are extracted by the MSOGI.

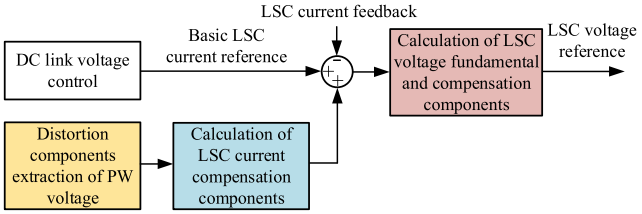

FIGURE 23. Compensation method based on LSC for standalone BDFIG under special loads.

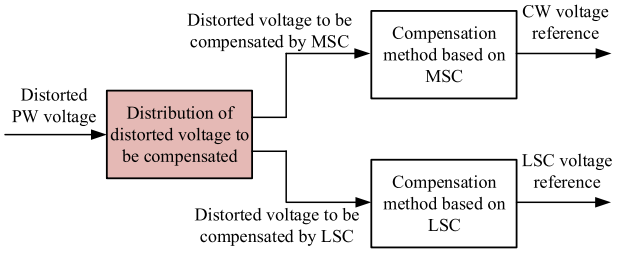

FIGURE 24. Compensation method based on the collaborative control of MSC and LSC for standalone BDFIG under special loads.

B. COMPENSATION BASED ON DUAL POWER CONVERTERS

Although these single power converter-based methods introduced in the last section can achieve voltage distortion compensation under special loads, they require a higher power converter capacity. However, in practical applications, the converter capacity is limited to some extent. In order to eliminate voltage distortion as much as possible under the limited converter capacity, the collaborative control of MSC and LSC has been developed to optimize the system performance, whose basic principle can be seen in Fig. 24. This method can dynamically distribute the distorted PW voltage to be compensated between MSC and LSC according to the limitations of the capacities, voltages, currents and IGBT junction temperatures of the two power converters. And then, the MSC and LSC still adopt the compensation methods shown in Fig. 22 and Fig. 23, respectively.

In [80], considering the limitation of the rated voltage of the power converters, the MSC is responsible to eliminate the 7th harmonic components of PW voltage, and the LSC is used to suppress the negative-sequence and 5th harmonic components of PW voltage, when the standalone BDFIG supplying unbalanced and nonlinear loads.

In [81], a real-time and flexible assignment method of PW harmonic voltage elimination tasks between MSC and LSC has been developed. A weight factor is proposed to dynamically adjust the contribution of the two power converters on harmonics elimination, according to one or more constraint conditions, e.g., overheat, overcurrent, overvoltage, and so on. Hence, on the premise of ensuring safety, the capacity of each inverter is expected to be fully utilized to mitigate harmonics. If the weight factor is set to 1, all harmonics would be compensated by MSC. And, if the weigh factor is equal to 0, all harmonics would be compensated by LSC. Otherwise, both MSC and LSC would be utilized to suppress all the harmonics. The typical experimental results, carried out a 30 kVA BDFIG under nonlinear loads, can be seen in Fig. 25. The weight factor is reduced from 1 to 0.2 step by step to test the system characteristics.

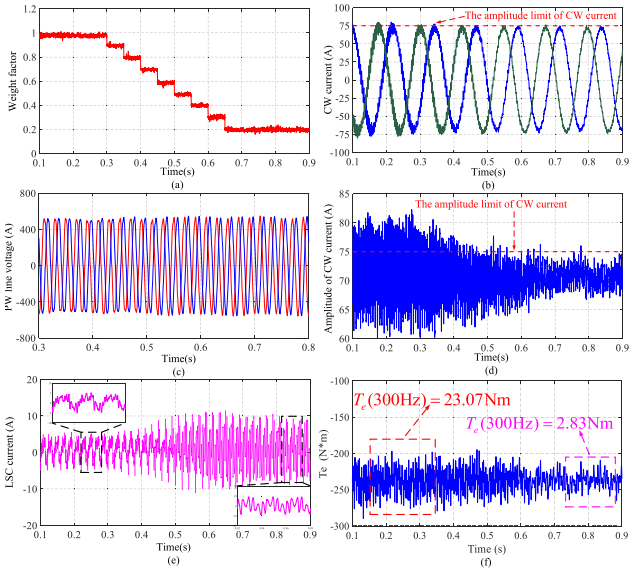

FIGURE 25. Experimental results of the compensation method based on the collaborative control of MSC and LSC with the weight factor reduction from 1 to 0.2 [81]. (a) Weight factor. (b) CW current. (c) PW line voltage. (d) Amplitude of CW current. (e) LSC current. (f) Electromagnetic torque.

As illustrated in Fig. 25, with the decrease of the weight factor, both the harmonics and amplitude of the CW current are reduced, while those of the LSC current are with the opposite trend. In addition, the electromagnetic torque ripple goes down along with the reduction of the weight factor. In the future, it is necessary to develop optimization algorithms

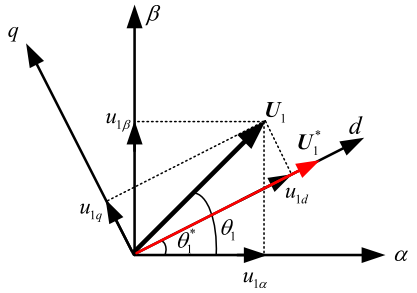

FIGURE 26. The actual and reference PW voltage vectors in the rotating dq reference frame [82].

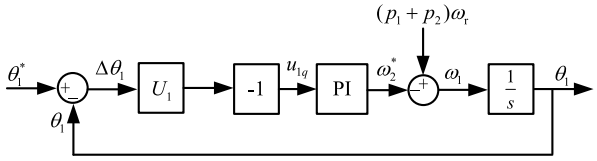

FIGURE 27. The structure of the linearized control loop for tracking the PW voltage phase in [82].

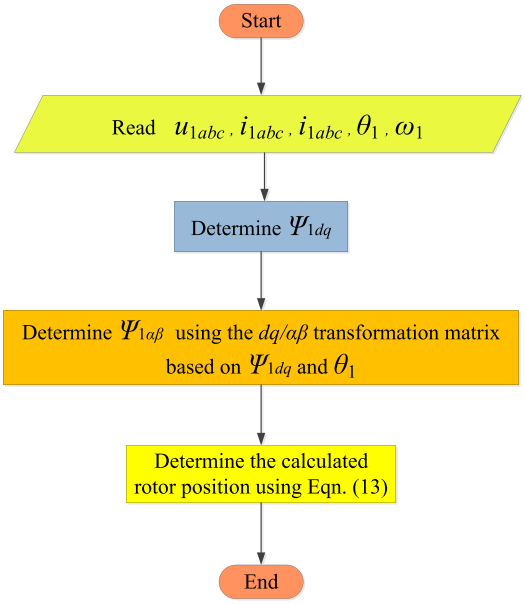

FIGURE 28. Flowchart of the direct calculation approach for BDFIG rotor position as developed in [86] and [87].

for automatically searching the optimal weight factor under different constraint conditions.

Table 5 shows the attribute comparison of the different compensation methods based on single power converter (MSC or LSC) and dual power converters. From Table 5, it can be concluded that the compensation method based on dual power converters is one of the most promising methods for BDFG-based standalone ac power generation under unbalanced and nonlinear loads

VI. SENSORLESS CONTROL

Lots of control techniques for BDFGs are based on the information of the generator rotor speed/position. However, the existence of the rotor speed/position sensor in the control system is becoming undesirable, due to its associated problems such as the additional maintenance cost, and the reliability reduction. Therefore, the control methods without any rotor speed/position sensors are very essential for high-performance BDFG systems to improve the reliability and reduce the overall cost. The current research works on this topic mainly focus on the control methods without speed observer and the ones with speed observer.

TABLE 5. Comparison among compensation methods based on MSC, LSC, and dual power converters.

Attribute	MSC compensation	LSC compensation	Dual power converters compensation
Does it need extra load current sensors?	No	Yes	No
Can it eliminate the torque ripple?	No	Yes	Yes
Can it allocate of the harmonic mitigation task between the two power converters?	No	No	Yes

A. WITHOUT SPEED OBSERVER

In [82], a sensorless direct voltage control (DVC) method without the speed observer has been developed for standalone BDFIGs, which utilizes the principle of the *dq*-frame phase-locked loop (PLL) proposed in [83]. It achieves the sensorless control function by adjusting the CW current frequency to track the PW voltage phase, so that it is not necessary to estimate the rotor speed or position. The principle of this method can be introduced as follows.

In the control method proposed in [82], the *d*-axis of the rotating *dq* reference frame is aligned with the reference PW voltage vector, as shown in Fig. 26. Hence, the *q*-axis PW voltage can be expressed as

$$u_{1q} = U_1 \sin(\theta_1 - \theta_1^*) \tag{9}$$

where U_1 and U_1^* are the amplitudes of the actual and reference PW voltage vectors, θ_1 and θ_1^* are the phase angles of the actual and reference PW voltage vectors, respectively.

Around the equilibrium point, (9) can be simplified as

$$u_{1q} \approx U_1(\theta_1 - \theta_1^*) = -U_1\Delta\theta_1 \tag{10}$$

where $\Delta\theta_1$ is the difference between the reference phase angle and actual phase of the PW voltage.

If the u_{1q} is equal to zero, the actual and reference PW voltage vectors would be with the same phase angle. Besides, for the BDFIG, the CW current frequency can regulate the PW voltage frequency, thus adjusting the PW voltage phase. Hence, a PI controller can be employed to control u_{1q}, and the output of the PI controller is the reference value of the CW current frequency. The linearized control loop for regulating the PW voltage phase can be seen in Fig. 27, which is similar to the *dq*-frame PLL.

The advantages of the sensorless DVC method presented in [82] are that the implementation process is simple and

the machine parameters are not required. However, from the experimental results, it can be seen that the PW voltage phase is with a steady-state error during the rapid change of the rotor speed. The sensorless DVC method has been successfully used in the sensorless phase control of PW voltage for standalone BDFIGs under unbalanced loads [84].

B. WITH SPEED OBSERVER

The estimation approaches of the current BDFG speed observers mainly include the direct calculation approaches and the closed-loop estimation approaches, which will be introduced in detail as follows.

1) DIRECT CALCULATION APPROACHES

The direct calculation approaches for BDFIG rotor position have been investigated in [85]–[87]. Generally, no PI controllers are required in these direct calculation approaches, and consequently a good starting performance can be obtained. Besides, there are no control parameters to be tuned so that the algorithm implementation is easy. However, the dependence on machine parameters will degrade the robustness of these approaches.

In [85], the CW back-EMF is integrated to obtain the CW flux in $\alpha\beta$ frame at first, and then the position angle of the CW flux can be obtained by

$$\theta_{2\_\mathrm{flux}} = \tan^{-1}\left(\psi_{2\beta}/\psi_{2\alpha}\right). \tag{11}$$

And then, the PW flux in $\alpha\beta$ frame also can be derived by the similar method. Afterwards, using a rotational transformation to the fixed rotor frame, the estimated rotor position can be obtained by

$$\hat{\theta}_r = \frac{\angle\left(\mathrm{e}^{-\mathrm{j}\theta_{2\_\mathrm{flux}}}\boldsymbol{\psi}_{1\alpha\beta}\right)}{p_1 + p_2} \tag{12}$$

Due to the usage of PW and CW flux, the accurate 3-phase voltages and currents of PW and CW need to be measured, and the PW and CW resistances should be known. Besides, the pure integrators are not directly suitable for experimental implementation of the PW and CW flux calculation, because of unavoidable dc-offsets in the measured voltages and currents.

In [86] and [87], the proposed approach needs the knowledge of the PW flux, and the PW and CW currents. In order to eliminate the integration process for calculating the PW flux, the dq-axis PW flux is calculated at first and then transformed to the $\alpha\beta$-axis quantities. Finally, the estimated rotor position can be obtained by

$$\hat{\theta}_r = \tan^{-1}\frac{\left(\psi_{1\alpha} - A_p i_{1\alpha}\right) i_{2\beta} + \left(\psi_{1\beta} - A_p i_{1\beta}\right) i_{1\alpha}}{\left(\psi_{1\alpha} - A_p i_{1\alpha}\right) i_{2\alpha} - \left(\psi_{1\beta} - A_p i_{1\beta}\right) i_{2\beta}} \tag{13}$$

where $A_p = L_1 - L_{1r}^2/L_r$.

It can be found that the calculation process shown in Fig. 28 is easy to implement in the digital signal processor. Furthermore, no integrators are required, which would significantly reduce the cumulative error of the estimated rotor position.

2) CLOSED-LOOP ESTIMATION APPROACHES

The closed-loop estimation means that the estimated rotor speed/position needs to be feedbacked to the speed observer for improving the estimation accuracy. Generally, this kind of approaches are with the higher estimation accuracy than the direct calculation approaches. However, the starting performance of the closed-loop estimation approaches are worse than that of the direct calculation approaches. Since some control parameters have to be tuned, the algorithm implementation of the closed-loop estimation approaches is more difficult than of the direct calculation approaches.

• *Speed Observers Dependent on Machine Parameters*

In [88] and [89], a quasi-closed-loop estimation approach is proposed for the BDFRG, which is the combination of the direct calculation and the closed-loop estimation. At first, the raw value of the rotor position is derived by the direct calculation approach. And then, the raw rotor position is sent to a Luenberger type closed-loop PI observer for filtering out erroneous signals and it can obtain the accurate rotor speed. The sensorless control methods with the principle of model reference adaptive system (MRAS) have attracted great attention from researchers for its high-performance operation.

The MRAS speed observers have been applied to DFIGs [90]–[95] and also been extended to the applications of BDFGs with different control state variables [96]–[102]. According to the control state variables, these MRAS speed observers presented in [96]–[102] can be divided to three groups, i.e., the observers based on CW current, the ones based on CW flux, and the ones based on CW power.

In [96] and [97], the MRAS speed observers have been developed with the CW current served as the control state variable. And, the stator flux is also required in these observers, so that the integration process has to be used. However, the integration process is susceptible to the dc-offsets in the sampled PW and CW back-EMFs, and would slow down the response speed at the system startup.

In order to avoid the integration process for the flux estimation, the MRAS speed observers employing the dq-axis CW flux as the control state variable have been proposed for sensorless control of BDFRG and BDFIG in [98] and [99], respectively.

Without the integration operation for the flux estimation, some other improved MRAS speed observers based on the CW active/reactive/fictitious power (CW-$P/Q/X$ MRAS) as the control state variables, as shown in Fig. 29, have been investigated for standalone BDFIGs in [100]–[102]. The main innovation of these MRAS observers presented in [100]–[102] is to eliminate the integration process for the flux estimation and reduce the voltage sensors used to detect the CW dq-axis components. Moreover, the presented simulation and experimental results have ensured the functionality of the adopted MRAS method to effectively estimate the rotor position with a good tracking under various operating states of both speed and load changes.

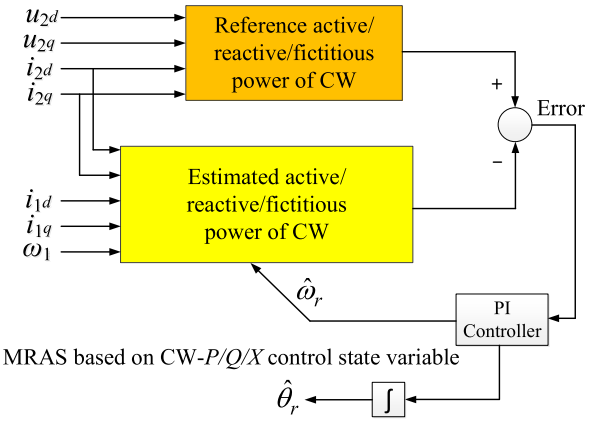

FIGURE 29. Structure of the proposed CW-*P*/*Q*/*X* MRAS speed observers for standalone BDFIGs [100]–[102].

• *Machine-Parameter-Free Speed Observers*

All the closed-loop estimation approaches mentioned above are severely dependent on the machine parameters, which would degrade the system robustness against the machine parameter mismatch. In order to address this issue, some typical machine-parameter-free speed observers have been developed for standalone BDFIG [103]–[105].

The basic machine-parameter-free speed observer (MPFSO), as shown in Fig. 30(a), has been proposed in [103] according to the following principle.

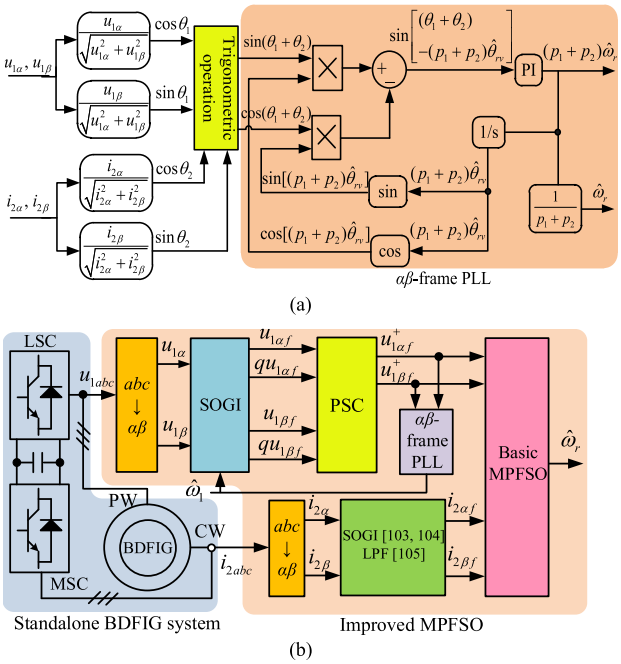

FIGURE 30. Structures of the machine-parameter-free speed observers (MPFSOs). (a) Structure of the basic MPFSO [103]. (b) Structure of the improved MPFSO [103]–[105].

It is well known that the mechanical rotor speed of BDFIG can be decided by

$$(p_1 + p_2)\omega_r = \omega_1 + \omega_2. \tag{14}$$

If one integrates (14), with ignoring the initial value of the integral operation, the following expression can be obtained:

$$(p_1 + p_2)\theta_{rv} = \theta_1 + \theta_2 \tag{15}$$

where θ_1 and θ_2 are the phase angles of PW voltage and CW current, respectively, and θ_{rv} can be regarded as the virtual rotor position, i.e., an intermediate variable for calculating the rotor speed.

Based on the small signal analysis method, the difference between the actual and estimated virtual rotor positions, $\Delta\theta_{rv}$, can be expressed as

$$\begin{aligned}(p_1 + p_2)\Delta\theta_{rv} &= (p_1 + p_2)(\theta_{rv} - \hat{\theta}_{rv}) \\ &= (\theta_1 + \theta_2) - (p_1 + p_2)\hat{\theta}_{rv} \\ &\approx \sin[(\theta_1 + \theta_2) - (p_1 + p_2)\hat{\theta}_{rv}]. \end{aligned} \tag{16}$$

According to the principle of the $\alpha\beta$-frame PLL presented in [106], $\Delta\theta_{rv}$ can converge to zero by using a PI controller, and the output of the PI controller would be the accurately estimated rotor speed.

However, under unbalanced and nonlinear loads, the standalone BDFIG suffers from the distorted PW voltage and CW current, which results in the inaccurate rotor speed estimation. To solve this problem, the improved MPFSOs have been proposed in [103]–[105], with using appropriate filters to eliminate the distorted components in PW voltage and CW current generated by unbalanced and nonlinear loads.

In [103] and [104], the improved MPFSO utilizes the second-order generalized integrators (SOGIs) to filter the harmonics in PW voltage and CW current, and employs the positive-sequence calculator (PSC) to eliminate the negative-sequence components in PW voltage, as shown in Fig. 30(b). Afterwards, the filtered PW voltage and CW current are sent to the basic MPFSO for deriving the accurate rotor speed.

It can be noted that when the BDFIG operates at its natural synchronous speed, the CW frequency should be set to zero to keep constant PW frequency. Hence, the filtering performance of the low-pass filter (LPF) would be better that that of the SOGI for CW current around the natural synchronous speed. Consequently, the improved MPFSO presented in [105] employs LPFs to eliminate the impact of unbalanced and nonlinear loads on the CW current. In addition, the parameter tunning guideline for the improved MPFSO has been designed for various operation conditions. As can be seen from Fig. 31, under the most severe load condition (the unbalanced nonlinear load), the ripple in the rotor speed obtained by the improved MPFSO can be significantly reduced, with almost the same response speed as the basic MPFSO. The defect of the improved MPFSO is that the parameter tunning requires the knowledge of the speed range.

TABLE 6 shows the attribute comparison of different sensorless control methods, in terms of starting performance, transient performance, estimation accuracy, robustness to machine parameters and ease of implementation. From this table, it can be concluded that the sensorless control methods

based on closed-loop speed/position estimation have the best overall drive performance.

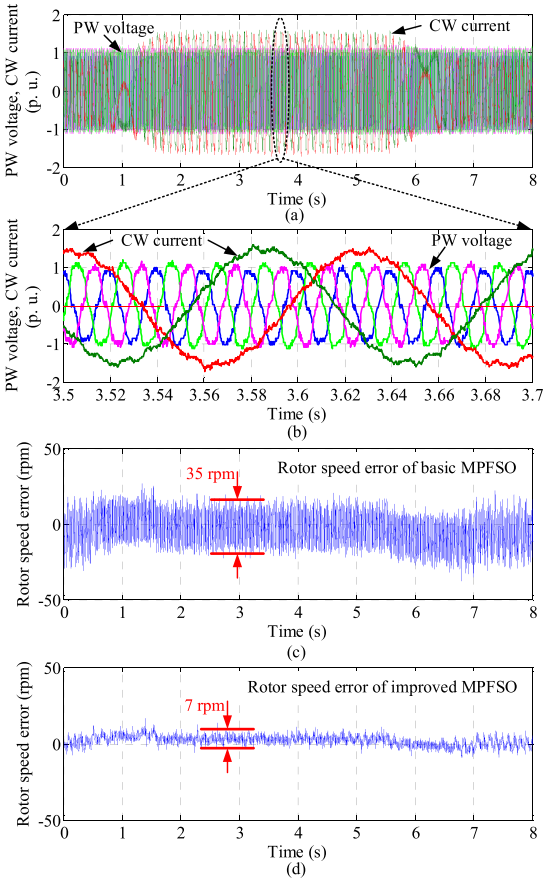

FIGURE 31. Comparison of the experimental results between the basic and improved MPFSOs under the unbalanced nonlinear load [105].

TABLE 6. Comparison of different sensorless control methods.

Attribute	Without speed observer	Direct speed/position estimation	Closed-loop speed/position estimation
Starting performance	Medium	High	Medium
Transient performance	Medium	Low	High
Estimation accuracy	Null	Medium	High
Robustness to machine parameters	Medium	Low	High
Ease of implementation	Medium	High	Low

VII. DC POWER GENERATION

The BDFG-based dc power generation system is originated from the corresponding DFIG system. In the last ten years, the research work on the DFIG-based dc power generation has been carried out, including coordinated control [107], [108], sensorless control [109], efficiency optimization control [110], direct torque control [111], torque ripple rejection [112], stator frequency regulation [113], [114], and power control [115], [116].

Recently, the BDFG-based dc power generation system has also attracted much attention [14], [117], [118]. Compared to the conventional BDFG ac system, the BDFG dc system can offer a novel solution to integrate the BDFG into the dc transmission system with the simpler topology, the better performance and the lower cost.

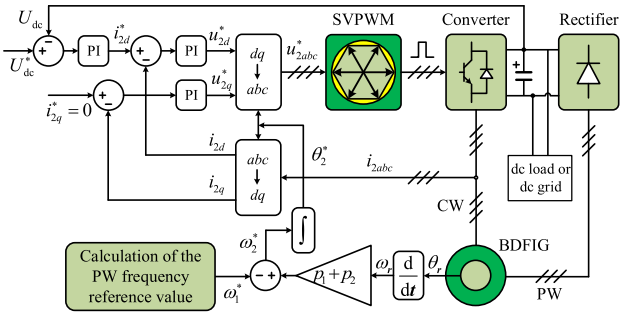

FIGURE 32. The basic control topology of the BDFG-based dc power generation system [14].

The basic control topology of the BDFIG-based dc power generation system is shown in Fig. 32 [14]. The PW can charge the dc bus capacitors through the rectifier, while the CW is controlled by the power converter to regulate the PW voltage and frequency. The speed encoder is used to achieve the rotor speed. Combining the reference value of the PW frequency, the angle of the frame transformation for the CW voltage and current can be derived. With the additional control freedom, the PW frequency is not limited to its rated value and can be regulated to achieve other purposes, e.g. efficiency optimization.

In [14], in order to improve the efficiency of the BDFIG-based dc power generation system, the PW frequency is no longer constant in the entire speed range. At the super-synchronous speed, the PW frequency is kept at its rated value $\omega_{1\mathrm{N}}$. At the sub-synchronous speed, the PW frequency is related to the rotor speed and can be set to $(p_1 + p_2)\omega_r$. Hence, the reference value of the CW frequency can be set as

$$\begin{aligned} \omega_2 &= \omega_r(p_1 + p_2) - \omega_{1\mathrm{N}} \quad \text{if } \omega_r \geq \omega_{r\mathrm{N}} \\ \omega_2 &= 0 \quad \text{if } \omega_r \leq \omega_{r\mathrm{N}} \end{aligned} \tag{17}$$

where $\omega_{r\mathrm{N}}$ is the natural synchronous speed of the BDFIG.

From (17), it can be noted that the CW frequency would be not less than zero, so that the CW hardly absorbs power in the full speed range. Consequently, the system efficiency can be improved.

In [117], based on the improved steady-state equivalent circuit considering the iron loss, the relationship between the efficiency and PW frequency is analyzed. From the obtained relationship, the optimal PW frequency for maximum efficiency can be achieved. This means that the operation mode of BDFIG can be changed from the constant-frequency-constant-voltage (CFCV) mode to the variable-frequency-constant-voltage (VFCV) mode in order to obtain the maximum efficiency. The efficiency optimization method based on the VFCV mode can be applied to BDFIG DC systems for the ship-shaft and wind power generation, since

the PW frequency of the dc power generation system is with the additional freedom of control.

From [117], the efficiency of the BDFIG can be depicted as

$$\eta = \frac{U_{\mathrm{dc}} I_{\mathrm{load}}}{\left[\begin{array}{l} U_{\mathrm{dc}} I_{\mathrm{load}} + \left(\frac{k_1}{\omega_1^2} + \frac{k_2}{\omega_1}\right) U_{\mathrm{dc}}^2 + \left(\frac{k_3}{\omega_1} + k_4\right) U_{\mathrm{dc}} I_2 \\ + \left(k_5 + k_6 \omega_1\right) I_2^2 \end{array}\right]} \quad (18)$$

where U_{dc} is the dc bus voltage, I_{load} and I_2 are the phase current RMS values of the load and the CW, respectively. The coefficients, k_1, k_2, k_3, k_4, k_5 and k_6, are related to the machine parameters.

From (18), the optimal PW angular frequency ω_{1_opt} can be obtained by solving the following equation

$$k_6 I_2^2 \omega_{1\_\mathrm{opt}}^3 - \left(k_2 U_{\mathrm{dc}}^2 + k_3 U_{\mathrm{dc}} I_2\right) \omega_{1\_\mathrm{opt}} - 2 k_1 U_{\mathrm{dc}}^2 = 0. \quad (19)$$

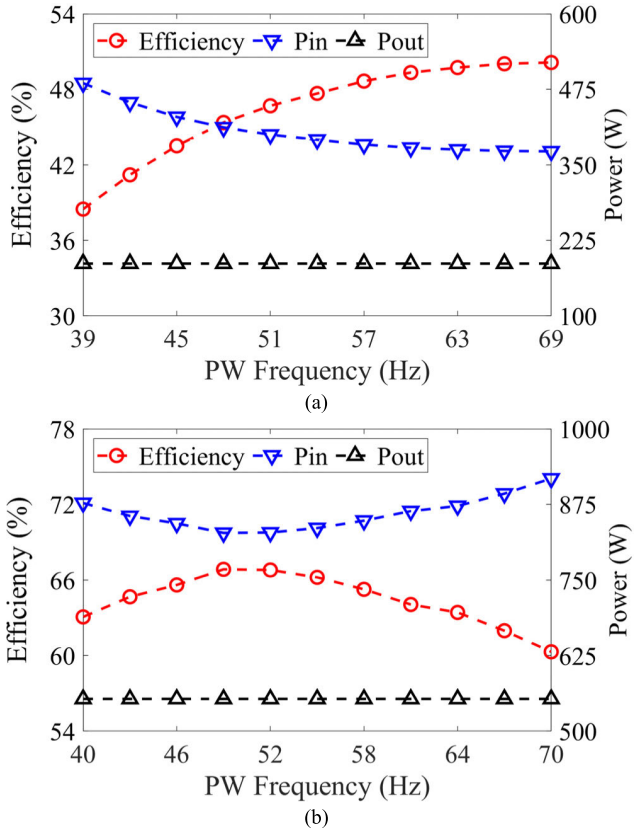

FIGURE 33. The experimental results of the BDFIG efficiency under different PW frequencies [117]. (a) The results with the load of 190 W at the sub-synchronous speed of 720 rpm. (b) The results with the load of 550 W at the super-synchronous speed of 780 rpm.

The typical experimental results, carried out a 5 kVA BDFIG-WR, can be seen in Fig. 33 [117]. Under the load power of 190 W and the sub-synchronous speed of 720 rpm, the efficiency of the BDFIG increases monotonically as the PW frequency varies from 39 to 69 Hz, as shown in Fig. 33(a). And, under the load power of 550 W and the super-synchronous speed of 780 rpm, the efficiency increases at first

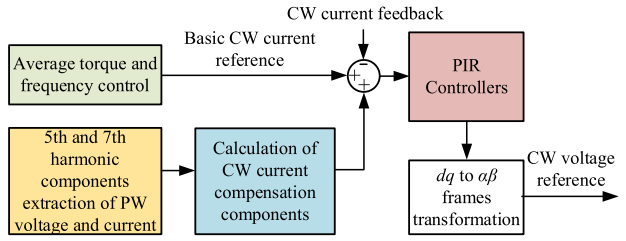

FIGURE 34. Block diagram of the torque ripple rejection method for the BDFIG-based dc power generation system proposed in [118].

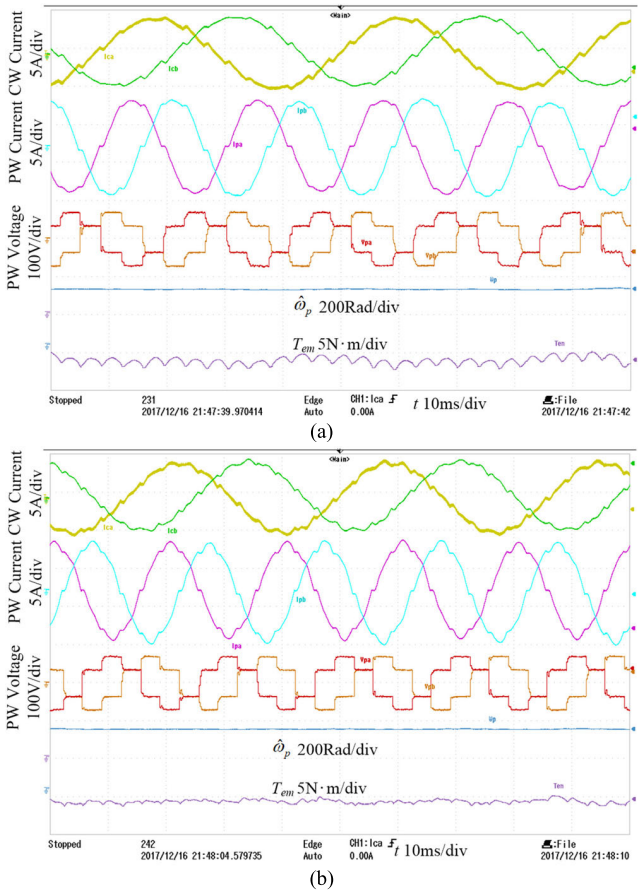

FIGURE 35. The experimental results of the torque ripple rejection method proposed in [118]. (a) Without torque ripple rejection. (b) With torque ripple rejection.

and then decreases as the PW frequency varies from 40 to 70 Hz, as shown in Fig. 33(b).

In the BDFIG-based dc power generation system, the diode rectifier connected to the PW inevitably produces distorted PW voltage and current, which results in considerable torque ripples. In order to address this issue, a torque ripple rejection method has been investigated in [118]. This method mainly eliminates the 6th harmonic torque caused by the 5th and 7th harmonic components of PW voltage and current through injecting harmonic current to CW, as shown in Fig. 34.

The corresponding experimental results is obtained in 10 kW DSBDFIG prototype, as shown in Fig. 35. From Fig. 35, it is noted that the ratio of the torque ripple can be

reduced from 9.2% to 1.4% with the torque ripple rejection strategy.

VIII. CONCLUSION AND PROSPECTS

This paper presents recent advances of BDFG control technologies, especially for grid-connected and standalone ac power generation, senslorless control and dc power generation. TABLE 7 summarizes the BDFG types that the various control methods are investigated against. It can be noted that few papers deal with the control methods of the BDFG-HR. To the best knowledge of the authors, the current research on the BDFG-HR mainly focuses on the machine design, performance analysis, modelling and loss estimation [10], [119]–[126].

TABLE 7. The BDFG types that various control methods are investigated against.

Operation conditions	Control methods	Machine types
Grid-connected ac power generation under normal grid	Vector control	BDFIG-NLR, BDFIG-WR, BDFRG, CDFIG
	Direct control	BDFIG-NLR, BDFIG-WR, BDFRG, CDFIG
	Indirect control	BDFIG-NLR
Grid-connected ac power generation under faulty grids	UGRT	BDFIG-NLR, DSBDFIG, CDFIG
	LVRT	BDFIG-NLR, BDFIG-WR
Standalone ac power generation with normal loads	CW current control without decoupling	BDFIG-WR, DSBDFIG
	CW current control with decoupling	BDFIG-WR
	Predictive control for CW current	BDFIG-WR
Standalone ac power generation with special loads	Single-power-converter compensation	BDFIG-WR, DSBDFIG
	Dual-power-converter compensation	BDFIG-WR
——	Sensorless control without speed observer	BDFIG-WR
	Sensorless control with speed observer	BDFIG-NLR, BDFIG-WR, BDFRG
DC power generation	——	BDFIG-WR, DSBDFIG

Each section of the control technologies mentioned above can be summarized below.

1) For grid-connected ac power generation applications, the recent BDFG control technologies deal with the operation under both the normal and faulty grids. The control technologies under the normal grid mainly include the vector control, direct control and indirect control, among which the vector control is mostly studied. However, for the vector control, the dependence on machine parameters in terms of flux estimation and cross decoupling of d- and q-axes control loops is still a great challenge. The control technologies under the faulty grids are mainly for the UGRT and LVRT operation. The machine parameter mismatch is one of the most important causes that degrade the performance of the control strategies under faulty grids.
2) For standalone ac power generation applications, the research progress of the BDFG control technologies under normal and special loads is discussed in this paper. The CW current controller is one of the key elements for the standalone BDFG operation under normal loads, which can be divided into three main categories, i.e., the PI controller without decoupling, the PI controller with decoupling, and the predictive controller. The decoupling loop can improve the dynamic performance of the CW current controller. However, it depends on the machine parameters or load model. The predictive control may be a good way to improve the accuracy of CW current tracking, although its computational burden increases greatly. The control technologies under special loads mainly include the compensation control methods based on the single power converter and those based on the dual power converters. In order to eliminate the PW voltage distortion as much as possible under the limited converter capacity, the compensation method based on the dual power converters would be one of the most promising methods.
3) The currently proposed sensorless control methods include the ones without speed observer and the ones with speed observer. The method without speed observer is based on the principle of the *dq*-frame PLL and independent of machine parameters. However, the performance of this control method is degraded during the rapid rotor speed change. The developed BDFG speed observers mainly include the direct calculation approaches and the closed-loop estimation approaches. Compared with the direct calculation, the closed-loop rotor speed/position estimation is with the better overall performance in terms of starting performance, transient performance, estimation accuracy, robustness to machine parameters and ease of implementation.
4) The BDFIG-based dc power generation system has some inherent advantages, e.g., the relatively low power converter cost, the simple control target, and so on. In such system, the frequency of PW voltage is a free variable, which can be utilized to achieve more control objectives. Besides, the inherent torque ripple caused by the system structure is a challenge to practical applications. The variable PW frequency control has been studied to improve the system efficiency. And, the torque ripple rejection method has also been developed. However, some other important topics have not been investigated, such as speed range extension, sensorless control, and so on.

With the ongoing development of BDFG control technologies during the past ten years and to the best knowledge of the authors, the following research topics should deserve more research efforts in the future:

1) Identification of machine parameters. The accurate machine parameters can significantly enhance the dynamic performance of the BDFG control system and improve the estimation accuracy of the rotor speed/position observers.
2) Speed range extension and efficiency optimization control for BDFIG-based dc power generation system. The topology and control target of the BDFIG-based dc power generation system make the PW frequency a free variable, which provides possibilities for speed range extension and efficiency optimization.
3) Applications of BDFG to other promising industrial applications. BDFGs have been applied to grid-connected and standalone systems. The corresponding control technologies can be extended to some other promising industrial applications, such as the microgrid.

REFERENCES

[1] R. A. McMahon, P. C. Roberts, X. Wang, and P. J. Tavner, "Performance of BDFM as generator and motor," *Proc. Inst. Elect. Eng.-Elect. Power Appl.*, vol. 153, no. 2, pp. 289–299, Mar. 2006.
[2] W. Xu and Y. Liu, *Advanced Control Technologies for Brushless Doubly-Fed Induction Machine*. Beijing, China: China Machine Press, 2020, pp. 5–9.
[3] T. D. Strous, H. Polinder, and J. A. Ferreira, "Brushless doubly-fed induction machines for wind turbines: Developments and research challenges," *IET Elect. Power Appl.*, vol. 11, no. 6, pp. 991–1000, Jul. 2017.
[4] P. Han, M. Cheng, S. Ademi, and M. G. Jovanovic, "Brushless doubly-fed machines: Opportunities and challenges," *Chin. J. Elect. Eng.*, vol. 4, no. 2, pp. 1–17, Jun. 2018.
[5] S. Williamson, A. C. Ferreira, and A. K. Wallace, "Generalised theory of the brushless doubly-fed machine. Part 1: Analysis," *IEE Proc.-Electr. Power Appl.*, vol. 144, no. 2, pp. 111–122, 1997.
[6] S. Williamson, A. C. Ferreira, and A. K. Wallace, "Generalised theory of the brushless doubly-fed machine. Part 2: Model verification and performance," *IEE Proc.-Electr. Power Appl.*, vol. 144, no. 2, pp. 123–129, 1997.
[7] R. E. Betz and M. G. Jovanovic, "Theoretical analysis of control properties for the brushless doubly fed reluctance machine," *IEEE Trans. Energy Convers.*, vol. 17, no. 3, pp. 332–339, Sep. 2002.
[8] A. M. Knight, R. E. Betz, and D. G. Dorrell, "Design and analysis of brushless doubly fed reluctance machines," *IEEE Trans. Ind. Appl.*, vol. 49, no. 1, pp. 50–58, Jan. 2013.
[9] F. Xiong and X. Wang, "Design of a low-harmonic-content wound rotor for the brushless doubly fed generator," *IEEE Trans. Energy Convers.*, vol. 29, no. 1, pp. 158–168, Mar. 2014.
[10] S. Yu, Y. Zhang, C. Chen, F. Zhang, and H. Nian, "Loss estimation of brushless doubly-fed generator with hybrid rotor considering multiple influence factors," *IEEE Access*, vol. 8, pp. 60043–60051, 2020.
[11] P. Han, M. Cheng, X. Wei, and N. Li, "Modeling and performance analysis of a dual-stator brushless doubly fed induction machine based on spiral vector theory," *IEEE Trans. Ind. Appl.*, vol. 52, no. 2, pp. 1380–1389, Mar./Apr. 2016.
[12] Y. Liu, W. Ai, B. Chen, K. Chen, and G. Luo, "Control design of the brushless doubly-fed machines for stand-alone VSCF ship shaft generator systems," *J. Power Electron.*, vol. 16, no. 1, pp. 259–267, Jan. 2016.
[13] X. Wang, H. Lin, and Z. Wang, "Transient control of reactive current for line-side converter of brushless doubly fed induction generator in stand-alone operation," *IEEE Trans. Power Electron.*, vol. 32, no. 10, pp. 8193–8203, Oct. 2017.
[14] Y. Liu, Y. Lin, W. Xu, and G. Zhi, "A brushless doubly-fed generator system and its control method," China Patent 2020 11 100 918.5, Oct. 15, 2020.
[15] T. Logan, J. Warrington, S. Shao, and R. Mcmahon, "Practical deployment of the brushless doubly-fed machine in a medium scale wind turbine," in *Proc. Int. Conf. Power Electron. Drive Syst. (PEDS)*, Nov. 2009, pp. 470–475.
[16] J. Chen, X. Wang, T. Zhao, Z. Li, M. Kong, and P. Nie, "Application of brushless doubly-fed machine system in hydropower generation," in *Proc. 22nd Int. Conf. Electr. Mach. Syst. (ICEMS)*, Aug. 2019, pp. 1–4.
[17] D. Zhou and R. Spee, "Field oriented control development for brushless doubly-fed machines," in *Proc. Conf. Rec. IEEE Ind. Appl. Conf., 31st Annu. Meeting (IAS)*, San Diego, CA, USA, 1996, pp. 304–310.
[18] H. Shoudao, H. Keyuan, Z. Lawu, and L. Lieen, "A study of the control strategy on rotor field orientation for brushless doubly-fed machine," in *Proc. 3rd Int. Power Electron. Motion Control Conf. (IPEMC)*, Beijing, China, 2000, pp. 508–513.
[19] G. Esfandiari, M. Ebrahimi, and A. Tabesh, "Instantaneous torque control method with rated torque-sharing ratio for cascaded DFIMs," *IEEE Trans. Power Electron.*, vol. 32, no. 11, pp. 8671–8680, Nov. 2017.
[20] F. Barati, S. Shao, E. Abdi, H. Oraee, and R. Mcmahon, "Generalized vector model for the brushless doubly-fed machine with a nested-loop rotor," *IEEE Trans. Ind. Electron.*, vol. 58, no. 6, pp. 2313–2321, Jun. 2011.
[21] F. Barati, R. McMahon, S. Shao, E. Abdi, and H. Oraee, "Generalized vector control for brushless doubly fed machines with nested-loop rotor," *IEEE Trans. Ind. Electron.*, vol. 60, no. 6, pp. 2477–2485, Jun. 2013.
[22] L. Xu, L. Zhen, and E.-H. Kim, "Field-orientation control of a doubly excited brushless reluctance machine," *IEEE Trans. Ind. Appl.*, vol. 34, no. 1, pp. 148–155, Feb. 1998.
[23] S. Ademi and M. G. Jovanović, "Vector control methods for brushless doubly fed reluctance machines," *IEEE Trans. Ind. Electron.*, vol. 62, no. 1, pp. 96–104, Jan. 2015.
[24] S. Ademi, M. G. Jovanović, and M. Hasan, "Control of brushless doubly-fed reluctance generators for wind energy conversion systems," *IEEE Trans. Energy Convers.*, vol. 30, no. 2, pp. 596–604, Jun. 2015.
[25] M. G. Mousa, S. M. Allam, and E. M. Rashad, "Maximum power extraction under different vector-control schemes and grid-synchronization strategy of a wind-driven brushless doubly-fed reluctance generator," *ISA Trans.*, vol. 72, pp. 287–297, Jan. 2018.
[26] B. Hopfensperger, D. J. Atkinson, and R. A. Lakin, "Stator flux oriented control of a cascaded doubly-fed induction machine," *IEE Proc.-Electr. Power Appl.*, vol. 146, no. 6, pp. 597–605, 1999.
[27] B. Hopfensperger, D. J. Atkinson, and R. A. Lakin, "Combined magnetizing flux oriented control of the cascaded doubly-fed induction machine," *IEE Proc. Electr. Power Appl.*, vol. 148, no. 4, pp. 354–362, Jul. 2001.
[28] K. Protsenko and D. Xu, "Modeling and control of brushless doubly-fed induction generators in wind energy applications," *IEEE Trans. Power Electron.*, vol. 23, no. 3, pp. 1191–1197, May 2008.
[29] C. H. S. de Vasconcelos, A. C. Ferreira, and R. M. Stephan, "Stator flux orientation control of the cascaded doubly fed induction machine," in *Proc. IEEE 24th Int. Symp. Ind. Electron. (ISIE)*, Buzios, Brazil, Jun. 2015, pp. 548–553.
[30] S. Hu and G. Zhu, "A vector control strategy of grid-connected brushless doubly fed induction generator based on the vector control of doubly fed induction generator," in *Proc. IEEE Appl. Power Electron. Conf. Expo. (APEC)*, Long Beach, CA, USA, Mar. 2016, pp. 3310–3316.
[31] J. Poza, E. Oyarbide, D. Roye, and M. Rodriguez, "Unified reference frame dq model of the brushless doubly fed machine," *IEE Proc.–Elect. Power Appl.*, vol. 153, no. 5, pp. 726–734, Sep. 2006.
[32] J. Poza, E. Oyarbide, I. Sarasola, and M. Rodriguez, "Vector control design and experimental evaluation for the brushless doubly fed machine," *IET Electr. Power Appl.*, vol. 3, no. 4, pp. 247–256, Jul. 2009.
[33] S. Shao, E. Abdi, F. Barati, and R. Mcmahon, "Stator-flux-oriented vector control for brushless doubly fed induction generator," *IEEE Trans. Ind. Electron.*, vol. 56, no. 10, pp. 4220–4228, Oct. 2009.
[34] Z. S. Du and T. A. Lipo, "Dynamics and vector control of wound-rotor brushless doubly fed induction machines," in *Proc. IEEE Energy Convers. Congr. Expo. (ECCE)*, Pittsburgh, PA, USA, Sep. 2014, pp. 1332–1339.
[35] M. Kong and X. Wang, "Reactive power regulating of a wound rotor brushless doubly-fed motor," in *Proc. 19th Int. Conf. Electr. Mach. Syst. (ICEMS)*, Chiba, Japan, 2016, pp. 1–5.
[36] D. Zhou and R. Spee, "Synchronous frame model and decoupled control development for doubly-fed machines," in *Proc. Power Electron. Specialist Conf. (PESC)*, Taipei City, Taiwan, 1994, pp. 1229–1236.
[37] S. Huang and L. Youjie, "Study of the control strategy on rotor field orientation for brushless doubly-fed machine," *Trans. China Electrotech. Soc.*, vol. 17, no. 2, pp. 34–39, 2002.
[38] Z. Wang and J. Li, "Vector control system simulation of brushless doubly-fed machine based on dual synchronous coordinate system," *J. Shenyang Univ. Technol.*, vol. 30, no. 5, pp. 489–493, 2008.

[39] M. G. Jovanovic, R. E. Betz, and J. Yu, "The use of doubly fed reluctance machines for large pumps and wind turbines," *IEEE Trans. Ind. Appl.*, vol. 38, no. 6, pp. 1508–1516, Nov./Dec. 2002.

[40] F. Valenciaga and P. F. Puleston, "Variable structure control of a wind energy conversion system based on a brushless doubly fed reluctance generator," *IEEE Trans. Energy Convers.*, vol. 22, no. 2, pp. 499–506, Jun. 2007.

[41] Z. Wang, "Study on the mathematic model and vector control of doubly fed brushless machine based on slip-frequency rotating reference frame," Ph.D. dissertation, School Elect. Eng., Shenyang Univ. Technol., Shenyang, China, 2006.

[42] Z. Wang and N. Zhao, "Indirect magnetic field directional method of Brushless doubly-fed machine with wish reluctance rotor based on slip frequency rotating frame," in *Proc. Int. Conf. Electr. Mach. Syst.*, Wuhan, China, 2008, pp. 958–962.

[43] J. Hu, J. Zhu, and D. G. Dorrell, "A new control method of cascaded brushless doubly fed induction generators using direct power control," *IEEE Trans. Energy Conv.*, vol. 29, no. 3, pp. 771–779, Sep. 2014.

[44] R. Sadeghi, S. M. Madani, M. R. A. Kashkooli, and S. Ademi, "Super-twisting sliding mode direct power control of a brushless doubly fed induction generator," *IEEE Trans. Ind. Electron.*, vol. 65, no. 11, pp. 9147–9156, Nov. 2018.

[45] S. Jin, L. Shi, L. Zhu, T. Dong, F. Zhang, and W. Cao, "Performance comparison of direct power control for brushless doubly-fed wind power generator with different control winding structure," in *Proc. IEEE Transp. Electrific. Conf. Expo, Asia–Pacific (ITEC Asia–Pacific)*, Busan, South Korea, Jun. 2016, pp. 261–266.

[46] W. R. Brassfield, R. Spee, and T. G. Habetler, "Direct torque control for brushless doubly-fed machines," *IEEE Trans. Ind. Appl.*, vol. 32, no. 5, pp. 1098–1104, Sep. 1996.

[47] Y. Ge and N. Wu, "Direct torque control for brushless doubly-fed machine based on SVPWM," *Small Spec. Electr. Mach.*, vol. 39, no. 8, pp. 58–60, 2011.

[48] D. Casadei, G. Serra, and A. Tani, "Improvement of direct torque control performance by using a discrete SVM technique," in *Proc. Rec. 29th Annu. IEEE Power Electron. Spec. Conf. (PESC)*, Fukuoka, Japan, May 1998, pp. 997–1003.

[49] S. J. Fattahi and A. A. Khayyat, "Direct torque control of brushless doubly-fed induction machines using fuzzy logic," in *Proc. IEEE 9th Int. Conf. Power Electron. Drive Syst.*, Dec. 2011, pp. 619–624.

[50] X. Yao, L. Shi, and Q. Guo, "Brushless doubly-fed machine direct torque control based on fuzzy strategy," *J. Power Supply.*, vol. 11, no. 6, pp. 54–58, 2011.

[51] A. Zhang and Y. Zhang, "Direct torque control for brushless doubly-fed machine based on torque predict control strategy," *Electr. Mach. Control*, vol. 11, no. 4, pp. 326–330, 2007.

[52] J.-K. Kang and S.-K. Sul, "New direct torque control of induction motor for minimum torque ripple and constant switching frequency," *IEEE Trans. Ind. Appl.*, vol. 35, no. 5, pp. 1076–1082, Sep. 1999.

[53] L. Bing, L. Shi, L. Teng, and Z. Jia, "Duty ratio modulation direct torque control of brushless doubly-fed machines," *Automatika*, vol. 58, no. 4, pp. 479–486, Oct. 2017.

[54] Z. Ai-Ling, J. Wen-Xia, Z. Zan-Qiang, and W. Xin, "A study on indirect stator-quantities control strategy for brushless doubly-fed induction machine," in *Proc. Int. Conf. Electr. Mach. Syst.*, Aug. 2011, pp. 1–6.

[55] A. Zhang, X. Wang, W. Jia, and Y. Ma, "Indirect stator-quantities control for the brushless doubly fed induction machine," *IEEE Trans. Power Electron.*, vol. 29, no. 3, pp. 1392–1401, Mar. 2014.

[56] R. Zhao, A. Zhang, Y. Ma, X. Wang, J. Yan, and Z. Ma, "The dynamic control of reactive power for the brushless doubly fed induction machine with indirect stator-quantities control scheme," *IEEE Trans. Power Electron.*, vol. 30, no. 9, pp. 5046–5057, Sep. 2015.

[57] S. Shao, T. Long, E. Abdi, and R. A. McMahon, "Dynamic control of the brushless doubly fed induction generator under unbalanced operation," *IEEE Trans. Ind. Electron.*, vol. 60, no. 6, pp. 2465–2476, Jun. 2013.

[58] L. Xu, M. Cheng, X. Wei, X. Yan, and Y. Zeng, "Dual synchronous rotating frame current control of brushless doubly fed induction generator under unbalanced network," *IEEE Trans. Power Electron.*, vol. 36, no. 6, pp. 6712–6724, Jun. 2021.

[59] J. Chen, W. Zhang, B. Chen, and Y. Ma, "Improved vector control of brushless doubly fed induction generator under unbalanced grid conditions for offshore wind power generation," *IEEE Trans. Energy Convers.*, vol. 31, no. 1, pp. 293–302, Mar. 2016.

[60] M. Gholizadeh, S. Tohidi, A. Oraee, and H. Oraee, "Appropriate crowbar protection for improvement of brushless DFIG LVRT during asymmetrical voltage dips," *Int. J. Elect. Power Energy Syst.*, vol. 95, pp. 1–10, Feb. 2018.

[61] S. Tohidi, H. Oraee, M. R. Zolghadri, and P. J. Tavner, "Influence of different series dynamic resistors on low-voltage ride-through of brushless doubly fed induction generator," *Electr. Power Compon. Syst.*, vol. 43, nos. 8–10, pp. 995–1005, Jun. 2015.

[62] S. Tohidi, H. Oraee, M. R. Zolghadri, S. Shao, and P. Tavner, "Analysis and enhancement of low-voltage ride-through capability of brushless doubly fed induction generator," *IEEE Trans. Ind. Electron.*, vol. 60, no. 3, pp. 1146–1155, Mar. 2013.

[63] S. Tohidi, H. Oraee, M. R. Zolghadri, and M. Rahimi, "A control scheme to enhance low voltage ride-through of brushless doubly-fed induction generators," *Wind Energy*, vol. 19, no. 9, pp. 1699–1712, Sep. 2016.

[64] J. Huang and S. Li, "Analytical expression for LVRT of BDFIG with enhanced current control to CW and reactive power support from GSC," *Int. J. Electr. Power Energy Syst.*, vol. 98, pp. 243–255, Jun. 2018.

[65] T. Long, S. Shao, P. Malliband, E. Abdi, and R. A. McMahon, "Crowbarless fault ride-through of the brushless doubly fed induction generator in a wind turbine under symmetrical voltage dips," *IEEE Trans. Ind. Electron.*, vol. 60, no. 7, pp. 2833–2841, Jul. 2013.

[66] T. Long, S. Shao, E. Abdi, R. A. McMahon, and S. Liu, "Asymmetrical low-voltage ride through of brushless doubly fed induction generators for the wind power generation," *IEEE Trans. Energy Convers.*, vol. 28, no. 3, pp. 502–511, Sep. 2013.

[67] P. Nie, X. Wang, and M. Kong, "Dynamic analysis and oscillation elimination of brushless doubly fed wind power generation system during symmetrical voltage dips," *IET Renew. Power Gener.*, vol. 15, no. 2, pp. 267–277, Feb. 2021.

[68] A. Zhang, Z. Chen, R. Gao, J. Wang, Z. Ma, S. Wang, and Y. Wang, "Crowbarless symmetrical low-voltage ride through based on flux linkage tracking for brushless doubly fed induction generators," *IEEE Trans. Ind. Electron.*, vol. 67, no. 9, pp. 7606–7616, Sep. 2020.

[69] X. Wei, M. Cheng, W. Wang, P. Han, and R. Luo, "Direct voltage control of dual-stator brushless doubly fed induction generator for stand-alone wind energy conversion systems," *IEEE Trans. Magn.*, vol. 52, no. 7, pp. 1–4, Jul. 2016.

[70] Y. Liu, W. Ai, B. Chen, K. Chen, and G. Luo, "Control design and experimental verification of the brushless doubly-fed machine for stand-alone power generation applications," *IET Electr. Power Appl.*, vol. 10, no. 1, pp. 25–35, Jan. 2016.

[71] L. Sun, Y. Chen, L. Peng, Y. Zhang, and Y. Kang, "Control winding current-oriented control for stand-alone brushless doubly fed power generation system," in *Proc. IEEE Energy Convers. Congr. Expo. (ECCE)*, Montreal, QC, Canada, Sep. 2015, pp. 2776–2781.

[72] L. Sun, Y. Chen, J. Su, D. Zhang, L. Peng, and Y. Kang, "Decoupling network design for inner current loops of stand-alone brushless doubly fed induction generation power system," *IEEE Trans. Power Electron.*, vol. 33, no. 2, pp. 957–963, Feb. 2018.

[73] W. Xu, J. Gao, Y. Liu, and K. Yu, "Model predictive current control of brushless doubly-fed machine for stand-alone power generation system," in *Proc. 43rd Annu. Conf. IEEE Ind. Electron. Soc. (IECON)*, Beijing, China, Oct. 2017, pp. 322–327.

[74] J. Chen, Y. Liu, and W. Xu, "Nonparametric predictive current control for standalone brushless doubly-fed induction generators," in *Proc. Int. Conf. Electr. Mach. (ICEM)*, Aug. 2020, pp. 2189–2195.

[75] W. Xu, O. M. E. Mohammed, Y. Liu, and M. R. Islam, "Negative sequence voltage compensating for unbalanced standalone brushless doubly-fed induction generator," *IEEE Trans. Power Electron.*, vol. 35, no. 1, pp. 667–680, Jan. 2020.

[76] M. Cheng, Y. Jiang, P. Han, and Q. Wang, "Unbalanced and low-order harmonic voltage mitigation of stand-alone dual-stator brushless doubly fed induction wind generator," *IEEE Trans. Ind. Electron.*, vol. 65, no. 11, pp. 9135–9146, Nov. 2018.

[77] Y. Liu, W. Xu, J. Zhu, and F. Blaabjerg, "Sensorless control of standalone brushless doubly fed induction generator feeding unbalanced loads in a ship shaft power generation system," *IEEE Trans. Ind. Electron.*, vol. 66, no. 1, pp. 739–749, Jan. 2019.

[78] O. M. E. Mohammed, W. Xu, Y. Liu, and F. Blaabjerg, "An improved control method for standalone brushless doubly fed induction generator under unbalanced and nonlinear loads using dual-resonant controller," *IEEE Trans. Ind. Electron.*, vol. 68, no. 7, pp. 5594–5605, Jul. 2021.

[79] K. Yu, "Harmonics mitigation of standalone brushless doubly-fed induction generator under nonlinear loads," M.S. thesis, School Elect. Electron. Eng., Huazhong Univ. Sci. Technol., Wuhan, China, 2019.
[80] W. Xu, K. Yu, Y. Liu, and J. Chen, "Improved collaborative control of standalone brushless doubly fed induction generator under unbalanced and nonlinear loads considering voltage rating of converters," *IEEE Trans. Power Electron.*, vol. 35, no. 5, pp. 4959–4970, May 2020.
[81] W. Xu, K. Yu, Y. Liu, and J. Gao, "Improved coordinated control of standalone brushless doubly fed induction generator supplying nonlinear loads," *IEEE Trans. Ind. Electron.*, vol. 66, no. 11, pp. 8382–8393, Nov. 2019.
[82] Y. Liu, W. Xu, F. Xiong, and F. Blaabjerg, "Sensorless direct voltage control of the stand-alone brushless doubly-fed generator," in *Proc. 20th Int. Conf. Electr. Mach. Syst. (ICEMS)*, Sydney, NSW, Australia, Aug. 2017, pp. 1–6.
[83] S. K. Chung, "Phase-locked loop for grid-connected three-phase power conversion systems," *IEE Proc.-Electr. Power Appl.*, vol. 147, no. 3, pp. 213–219, May 2000.
[84] W. Xu, D. Dong, Y. Liu, K. Yu, and J. Gao, "Improved sensorless phase control of stand-alone brushless doubly-fed machine under unbalanced loads for ship shaft power generation," *IEEE Trans. Energy Convers.*, vol. 33, no. 4, pp. 2229–2239, Dec. 2018.
[85] U. Shipurkar, T. D. Strous, H. Polinder, J. A. Ferreira, and A. Veltman, "Achieving sensorless control for the brushless doubly fed induction machine," *IEEE Trans. Energy Convers.*, vol. 32, no. 4, pp. 1611–1619, Dec. 2017.
[86] W. Xu, M. G. Hussien, Y. Liu, M. R. Islam, and S. M. Allam, "Sensorless voltage control schemes for brushless doubly-fed induction generators in stand-alone and grid-connected applications," *IEEE Trans. Energy Convers.*, vol. 35, no. 4, pp. 1781–1795, Dec. 2020.
[87] M. G. Hussien, Y. Liu, and W. Xu, "Robust position observer for sensorless direct voltage control of stand-alone ship shaft brushless doubly-fed induction generators," *CES Trans. Electr. Mach. Syst.*, vol. 3, no. 4, pp. 363–376, Dec. 2019.
[88] M. G. Jovanovic and D. G. Dorrell, "Sensorless control of brushless doubly-fed reluctance machines using an angular velocity observer," in *Proc. 7th Int. Conf. Power Electron. Drive Syst.*, Nov. 2007, pp. 717–724.
[89] S. Ademi, M. G. Jovanović, H. Chaal, and W. Cao, "A new sensorless speed control scheme for doubly fed reluctance generators," *IEEE Trans. Energy Convers.*, vol. 31, no. 3, pp. 993–1001, Sep. 2016.
[90] M. F. Iacchetti, "Adaptive tuning of the stator inductance in a rotor-current-based MRAS observer for sensorless doubly fed induction-machine drives," *IEEE Trans. Ind. Electron.*, vol. 58, no. 10, pp. 4683–4692, Oct. 2011.
[91] R. Cardenas, R. Pena, J. Proboste, G. Asher, and J. Clare, "Rotor current based MRAS observer for doubly-fed induction machines," *Electron. Lett.*, vol. 40, no. 12, pp. 769–770, Jun. 2004.
[92] M. Pattnaik and D. Kastha, "Adaptive speed observer for a stand-alone doubly fed induction generator feeding nonlinear and unbalanced loads," *IEEE Trans. Energy Convers.*, vol. 27, no. 4, pp. 1018–1026, Dec. 2012.
[93] R. Cardenas, R. Pena, G. Asher, J. Clare, and J. Cartes, "MRAS observer for doubly fed induction machines," *IEEE Trans. Energy Convers.*, vol. 19, no. 2, pp. 467–468, Jun. 2004.
[94] R. Cardenas, R. Pena, J. Clare, G. Asher, and J. Proboste, "MRAS observers for sensorless control of doubly-fed induction generators," *IEEE Trans. Power Electron.*, vol. 23, no. 3, pp. 1075–1084, May 2008.
[95] R. Cardenas, R. Pena, J. Proboste, G. Asher, and J. Clare, "MRAS observer for sensorless control of standalone doubly fed induction generators," *IEEE Trans. Energy Convers.*, vol. 20, no. 4, pp. 710–718, Dec. 2005.
[96] M. He, Z. Wei, and X. Chen, "A sensor-less vector control of brushless doubly-fed machine for stand-alone generator system," in *Proc. 20th Int. Conf. Electr. Mach. Syst. (ICEMS)*, Sydney, NSW, Australia, Aug. 2017, pp. 1–5.
[97] J. Yang, W. Tang, G. Zhang, Y. Sun, S. Ademi, F. Blaabjerg, and Q. Zhu, "Sensorless control of brushless doubly fed induction machine using a control winding current MRAS observer," *IEEE Trans. Ind. Electron.*, vol. 66, no. 1, pp. 728–738, Jan. 2019.
[98] K. Kiran, S. Das, and A. Sahu, "Sensorless speed estimation and control of brushless doubly-fed reluctance machine drive using model reference adaptive system," in *Proc. IEEE Int. Conf. Power Electron., Drives Energy Syst. (PEDES)*, Dec. 2016, pp. 1–6.
[99] W. Xu, A. K. Ebraheem, Y. Liu, J. Zhu, M. G. Hussien, and O. M. E. Mohammed, "An MRAS speed observer based on control winding flux for sensorless control of stand-alone BDFIGs," *IEEE Trans. Power Electron.*, vol. 35, no. 7, pp. 7271–7281, Jul. 2020.
[100] M. G. Hussien, Y. Liu, W. Xu, and M. Dong, "Sensorless position control based on active power MRAS for ship shaft stand-alone BDFIGs," in *Proc. Int. Conf. Electr. Mach. (ICEM)*, Gothenburg, Sweden, Aug. 2020, pp. 2209–2215.
[101] W. Xu, M. G. Hussien, Y. Liu, and S. M. Allam, "Sensorless control of ship shaft stand-alone BDFIGs based on reactive-power MRAS observer," *IEEE J. Emerg. Sel. Topics Power Electron.*, vol. 9, no. 2, pp. 1518–1531, Apr. 2021.
[102] M. G. Hussien, Y. Liu, W. Xu, and J. Rodriguez, "Fictitious power based MRAS observer for sensorless control of stand-alone brushless doubly-fed induction Generators," in *Proc. IEEE 9th Int. Power Electron. Motion Control Conf. (IPEMC-ECCE Asia)*, Nanjing, China, Nov. 2020, pp. 3511–3518.
[103] Y. Liu, W. Xu, T. Long, and F. Blaabjerg, "A new rotor speed observer for stand-alone brushless doubly-fed induction generators," in *Proc. IEEE Energy Convers. Congr. Expo. (ECCE)*, Cincinnati, OH, USA, Oct. 2017, pp. 5086–5092.
[104] Y. Liu, W. Xu, J. Zhu, and F. Blaabjerg, "Sensorless control of standalone brushless doubly fed induction generator feeding unbalanced loads in a ship shaft power generation system," *IEEE Trans. Ind. Electron.*, vol. 66, no. 1, pp. 739–749, Jan. 2019.
[105] Y. Liu, W. Xu, T. Long, and F. Blaabjerg, "An improved rotor speed observer for standalone brushless doubly-fed induction generator under unbalanced and nonlinear loads," *IEEE Trans. Power Electron.*, vol. 35, no. 1, pp. 775–788, Jan. 2020.
[106] R. Teodorescu and F. Blaabjerg, "Flexible control of small wind turbines with grid failure detection operating in stand-alone and grid-connected mode," *IEEE Trans. Power Electron.*, vol. 19, no. 5, pp. 1323–1332, Sep. 2004.
[107] D. Xiang, L. Ran, J. R. Bumby, P. J. Tavner, and S. Yang, "Coordinated control of an HVDC link and doubly fed induction generators in a large offshore wind farm," *IEEE Trans. Power Del.*, vol. 21, no. 1, pp. 463–471, Jan. 2006.
[108] H. Nian and X. Yi, "Coordinated control strategy for doubly-fed induction generator with DC connection topology," *IET Renew. Power Gener.*, vol. 9, no. 7, pp. 747–756, Sep. 2015.
[109] S. Bayhan, S. Demirbas, and H. Abu-Rub, "Fuzzy-PI-based sensorless frequency and voltage controller for doubly fed induction generator connected to a DC microgrid," *IET Renew. Power Gener.*, vol. 10, no. 8, pp. 1069–1077, Sep. 2016.
[110] G. D. Marques and M. F. Iacchetti, "Field-weakening control for efficiency optimization in a DFIG connected to a DC-link," *IEEE Trans. Ind. Electron.*, vol. 63, no. 6, pp. 3409–3419, Jun. 2016.
[111] A. Gundavarapu, H. Misra, and A. K. Jain, "Direct torque control scheme for DC voltage regulation of the standalone DFIG-DC system," *IEEE Trans. Ind. Electron.*, vol. 64, no. 5, pp. 3502–3512, May 2017.
[112] G. D. Marques and M. F. Iacchetti, "Minimization of torque ripple in the DFIG-DC system via predictive delay compensation," *IEEE Trans. Ind. Electron.*, vol. 65, no. 1, pp. 103–113, Jan. 2018.
[113] G. D. Marques and M. F. Iacchetti, "Stator frequency regulation in a field-oriented controlled DFIG connected to a DC link," *IEEE Trans. Ind. Electron.*, vol. 61, no. 11, pp. 5930–5939, Nov. 2014.
[114] C. Wu, H. Nian, B. Pang, and P. Cheng, "Adaptive repetitive control of DFIG-DC system considering stator frequency variation," *IEEE Trans. Power Electron.*, vol. 34, no. 4, pp. 3302–3312, Apr. 2019.
[115] C. Wu, P. Cheng, Y. Ye, and F. Blaabjerg, "A unified power control method for standalone and grid-connected DFIG-DC system," *IEEE Trans. Power Electron.*, vol. 35, no. 12, pp. 12663–12667, Dec. 2020.
[116] C. Wu, D. Zhou, and F. Blaabjerg, "Direct power magnitude control of DFIG-DC system without orientation control," *IEEE Trans. Ind. Electron.*, vol. 68, no. 2, pp. 1365–1373, Feb. 2021.
[117] Y. Zhang, Y. Liu, W. Xu, and J. Rodriguez, "Efficiency analysis of brushless doubly-fed induction generator based on improved steady-state equivalent circuit," in *Proc. IEEE Energy Convers. Cong. Expo. (ECCE)*, Vancouver, BC, Canada, Oct. 2021.
[118] Y. Jiang, M. Cheng, P. Han, Q. Wang, and X. Wang, "Analysis and dynamic control of a dual-stator BDFIG-DC system supplying DC grid with minimized torque ripple through harmonic current injection," *IEEE Trans. Power Electron.*, vol. 34, no. 6, pp. 5388–5399, Jun. 2019.
[119] F. Zhang, S. Yu, X. Wang, H. Wang, and S. Jin, "Research of a novel brushless doubly-fed generator with hybrid rotor," *IEEE Trans. Appl. Supercond.*, vol. 26, no. 7, pp. 1–5, Oct. 2016.
[120] F. G. Zhang, S. Y. Yu, and X. P. Wang, "Magnetic field modulation analysis and experimental research of brushless doubly fed generator with hybrid rotor," in *Proc. IEEE Int. Conf. Appl. Supercond. Electromagn. Devices (ASEMD)*, Shanghai, China, Nov. 2015, pp. 110–111.

[121] F. Zhang, Y. Li, and X. Wang, "The design and FEA of brushless doubly-fed machine with hybrid rotor," in *Proc. Int. Conf. Appl. Supercond. Electromagn. Devices*, Chengdu, China, Sep. 2009, pp. 324–327.
[122] F. Zhang, X. Ju, and H. Liu, "Electromagnetic design of 5MW dual-stator brushless doubly-fed generator with hybrid rotor," in *Proc. IEEE Transp. Electrific. Conf. Expo, Asia–Pacific (ITEC Asia–Pacific)*, Busan, South Korea, Jun. 2016, pp. 832–836.
[123] X. Wang, F. Zhang, Q. Yang, and G. Liu, "Performance analysis on a novel brushless doubly fed machine with hybrid rotor structure," in *Proc. Int. Conf. Electr. Mach. Syst.*, Beijing, China, Aug. 2011, pp. 1–4.
[124] F. Zhang, Y. Wang, and S. Yu, "Improved E&S model for core loss calculation of brushless doubly fed machine with hybrid rotor," *IEEE Trans. Magn.*, vol. 54, no. 11, pp. 1–5, Nov. 2018.
[125] F. Zhang, Y. Song, S. Yu, S. Jin, and C. Gerada, "Influence of slot combination on performance of brushless doubly fed generator with hybrid rotor," *IEEE Trans. Magn.*, vol. 55, no. 11, pp. 1–6, Nov. 2019.
[126] F. Zhang, S. Song, G. Jia, and S. Jin, "Performance of brushless doubly-fed synchronous generator with hybrid rotor," in *Proc. Int. Conf. Electr. Mach. Syst. (ICEMS)*, Busan, South Korea, Oct. 2013, pp. 695–698.

YI LIU (Senior Member, IEEE) received the B.E. and M.E. degrees in automation and control engineering from Wuhan University of Science and Technology, Wuhan, China, in 2004 and 2007, respectively, and the Ph.D. degree in mechatronic engineering from the Huazhong University of Science and Technology, Wuhan, in 2016.

From March 2016 to June 2016, he was a Senior Research and Development Engineer with the Fourth Academy of the China Aerospace Science and Industry Group, Wuhan. From July 2016 to October 2019, he was a Postdoctoral Research Fellow with the State Key Laboratory of Advanced Electromagnetic Engineering and Technology, Huazhong University of Science and Technology, where he has been a Lecturer, since January 2020. His current research interests include multi-port electrical machines and drive systems.

Dr. Liu received one Best Paper Awards from the IEEE TRANSACTIONS ON ENERGY CONVERSION, in 2020. He is currently the Vice Chair of IEEE IES Wuhan Chapter, and an Associate Editor of IEEE TRANSACTIONS ON INDUSTRY APPLICATIONS.

MOHAMED G. HUSSIEN (Graduate Student Member, IEEE) was born in Zefta, Gharbeya, Egypt, in 1988. He received the B.Sc. and M.Sc. degrees in electrical engineering from the Department of Electrical Power and Machines Engineering, Faculty of Engineering, Tanta University, Tanta, Egypt, in 2011 and 2016, respectively, and the Ph.D. degree from the School of Electrical and Electronic Engineering, Huazhong University of Science and Technology, Wuhan, China, in 2020.

He is currently an Assistant Professor with the Department of Electrical Power and Machines Engineering, Faculty of Engineering, Tanta University. He has published scientific papers in both international conferences and high-quality SCI journals. His research interests include electrical machines analysis, electrical drives, electric vehicles, sensorless control, doubly-fed machines, power electronics, and renewable energy systems.

He is a member of the IEEE-IES Electric Machines Technical Committee and the IEEE-IES Technical Committee on Renewable Energy Systems. His paper has been selected as one of the best papers published in the period (2019–2020) in the IEEE TRANSACTIONS ON ENERGY CONVERSION in the "Power generations systems and grid interfaces" area. He has been serving as a Reviewer for both IEEE conferences and many IEEE journals, including IEEE ACCESS, IEEE TRANSACTIONS ON INDUSTRIAL ELECTRONICS, and IEEE TRANSACTIONS ON POWER ELECTRONICS. He is currently serving as an Editorial Board Member for the *International Research Journal of Innovations in Engineering and Technology* (IRJIET). He is also serving as a Guest Editor for a special issue in *IET Renewable Power Generation* journal.

WEI XU (Senior Member, IEEE) received the double B.E. and M.E. degrees from Tianjin University, Tianjin, China, in 2002 and 2005, respectively, and the Ph.D. degree from the Institute of Electrical Engineering, Chinese Academy of Sciences, in 2008, respectively, all in electrical engineering.

From 2008 to 2012, he was a Postdoctoral Fellow with the University of Technology Sydney, the Vice Chancellor Research Fellow with the Royal Melbourne Institute of Technology, Japan Science Promotion Society Invitation Fellow with Meiji University. Since 2013, he has been a Full Professor with the State Key Laboratory of Advanced Electromagnetic Engineering, Huazhong University of Science and Technology, China. He has more than 110 articles accepted or published in IEEE Journals, two edited books published by Springer Press, one monograph published by China Machine Press, and more than 150 invention patents granted or in pending, all in the related fields of electrical machines and drives. His research interests include design and control of linear/rotary machines.

He is a fellow of the Institute of Engineering and Technology (IET). He will serve as the General Chair for 2021 International Symposium on Linear Drives for Industry Applications (LDIA 2021) and the 2023 IEEE International Conference on Predictive Control of Electrical Drives and Power Electronics (PRECEDE 2023), Wuhan, China. He has served as an Associate Editor for several leading IEEE TRANSACTIONS and Journals, such as IEEE TRANSACTIONS ON INDUSTRIAL ELECTRONICS, IEEE TRANSACTIONS ON VEHICULAR TECHNOLOGY, IEEE TRANSACTIONS ON ENERGY CONVERSION, and so on.

SHIYI SHAO (Member, IEEE) received the B.Eng. and M.Phil. degrees from Shanghai Jiao Tong University, in 2003 and 2006, respectively, and the M.Phil. and Ph.D. degrees from the University of Cambridge, in 2007 and 2010, respectively, all in electrical engineering.

He is currently with Wuxi Silent Electric System Technology Company Ltd., as the Chief Technical Director, working on frequency converter system for marine application. His research interests include power electronics, ac drives, machine control systems, and renewable energy generation.

ESSAM M. RASHAD (Senior Member, IEEE) was born in Shebin El-Kom, Egypt, in 1960. He received the B.Sc. degree from the Department of Electric Power and Machines Engineering, Faculty of Engineering, Menoufia University, Egypt, in 1983, and the M.Sc. and Ph.D. degrees from the Faculty of Engineering, Alexandria University, Egypt, in 1987 and 1992, respectively.

From 1985 to 1990, he was an Offshore Electrical Engineer with Belayim Petroleum Company, Egypt. In 1992, he joined the Faculty of Engineering, Tanta University, Egypt, where he has been a Full Professor, since 2006. From February 2000 to August 2000, he was a Visiting Researcher with the Faculty of Engineering, Nagasaki University, Japan. In summer 2003, he was a Visiting Researcher with the Faculty of Engineering and Applied Science, Memorial University of Newfoundland, St. John's, Canada. From 2004 to 2009, he was the Head of the Electrical Technology Department, Buraydah College of Technology, Saudi Arabia. From 2011 to 2014, he was the Vice Dean for education and student affairs of the Faculty of Engineering, Tanta University. He was the Head of electrical power and machines engineering, from 2009 to 2011, and from 2014 to September 2020. He has published more than 160 technical conference and journal papers. His research interests include electrical machine analysis and design, electrical drives, power electronics, micro-grids, distributed generation, and renewable energy systems.

Prof. Rashad received the Outstanding Engineering Award for "Outstanding Contribution in the Electrical Power Engineering Education, Research and Industry" from IEEE-PES (Power and Energy Society), Egypt Chapter, in 2019. He was the General Chairman of the 21st International Middle East Power Systems Conference (MEPCON'2019), Cairo, in December 2019, and the Co-Chairman of the First IEEE Conference on Power Electronics and Renewable Energy, Aswan, Egypt, in October 2019.